

1 **Landsat and Sentinel-derived glacial lake dataset in the China-**
2 **Pakistan Economic Corridor from 1990 to 2020**

3
4 Muchu Lesi¹, Yong Nie^{1, *}, Dan H. Shugar², Jida Wang³, Qian Deng^{1, 4}, Huayong Chen¹,
5 Jianrong Fan¹

6
7 ¹Institute of Mountain Hazards and Environment, Chinese Academy of Sciences, Chengdu,
8 China.

9 ²Water, Sediment, Hazards, and Earth-surface Dynamics (waterSHED) Lab, Department of
10 Geoscience, University of Calgary, Alberta, T2N 1N4, Canada

11 ³Department of Geography and Geospatial Sciences, Kansas State University, Manhattan,
12 Kansas 66506, USA

13 ⁴University of Chinese Academy of Sciences, Beijing 100190, China

14
15
16
17 *Corresponding author, nieyong@imde.ac.cn
18
19

20 **Abstract.** The China-Pakistan Economic Corridor (CPEC) is one of the flagship projects of
21 the One Belt One Road Initiative, which faces threats from water shortage and mountain
22 disasters in the high-elevation region, such as glacial lake outburst floods (GLOFs). An up-to-
23 date high-quality glacial lake dataset with parameters such as lake area, volume and type,
24 which is fundamental to water resource and flood risk assessments, and predicting glacier-
25 lake evolutions, is still largely absent for the entire CPEC. This study describes a glacial lake
26 dataset for the CPEC using a threshold-based mapping method associated with rigorous
27 visual inspection workflows. This dataset includes (1) multi-temporal inventories for 1990,
28 2000, and 2020 produced from 30 m resolution Landsat images, and (2) a glacial lake
29 inventory for the year 2020 at 10 m resolution produced from Sentinel-2 images. The results
30 show that, in 2020, 2234 lakes were derived from the Landsat images, covering a total area of
31 $86.31 \pm 14.98 \text{ km}^2$ with a minimum mapping unit of 5 pixels (4500 m^2), whereas 7560 glacial
32 lakes were derived from the Sentinel-2 images with a total area of $103.70 \pm 8.45 \text{ km}^2$ with a
33 minimum mapping unit of 5 pixels (500 m^2). The discrepancy shows that Sentinel-2 is able to
34 detect a significant quantity of smaller lakes than Landsat due to its finer spatial resolution.
35 Glacial lake data in 2020 was validated by Google Earth-derived lake boundaries with a
36 median (\pm standard deviation) difference of $7.66 \pm 4.96 \%$ for Landsat-derived product and
37 $4.46 \pm 4.62 \%$ for Sentinel-derived product. The total number and area of glacial lakes from
38 consistent 30 m resolution Landsat images remain relatively stable despite a slight increase
39 from 1990 to 2020. A range of critical attributes have been generated in the dataset, including
40 lake types and mapping uncertainty estimated by an improved Hanshaw's equation. This
41 comprehensive glacial lake dataset has potential to be widely applied in studies on water
42 resource assessment, glacial lake-related hazards, glacier-lake interactions, and is freely
43 available at <https://doi.org/10.12380/Glaci.msdc.000001> (Lesi et al., 2022).

44 **1 Introduction**

45 Glaciers in High-mountain Asia (HMA) play a crucial role in regulating climate, supporting
46 ecosystems, modulating the release of freshwater into rivers, and sustaining municipal water
47 supplies (Wang et al., 2019; Viviroli et al., 2020), agricultural irrigation, and hydropower
48 generation (Pritchard, 2019; Nie et al., 2021). Most HMA glaciers are losing mass in the
49 context of climate change (Brun et al., 2017; Maurer et al., 2019; Shean et al., 2020;
50 Bhattacharya et al., 2021), therefore, unsustainable glacier melt and the passing of peak water
51 are reducing the hydrological role of glaciers (Huss and Hock, 2018) and impacting
52 downstream ecosystem services, agriculture, hydropower and other socioeconomic values
53 (Carrivick and Tweed, 2016; Nie et al., 2021). The present and future glacier changes not
54 only impact water supply for downstream area but also alter the frequency and intensity of
55 glacier-related hazards, such as glacier lake outburst floods (GLOFs) (Nie et al., 2018;
56 Rounce et al., 2020; Zheng et al., 2021), and rock and ice avalanches (Shugar et al., 2021).
57 Global glacial lake number and total area both increased between 1990 and 2018 in response
58 to glacier retreat and climate change (Shugar et al., 2020), affecting the allocation of
59 freshwater resource. The Indus is globally the most important and vulnerable water tower unit
60 where glaciers, lakes and reservoir storage contribute about two-thirds of the water supply
61 (Immerzeel et al., 2020). Ice-marginal lakes store $\sim 1\%$ of total ice discharge in Greenland and
62 accelerate lake-terminating ice velocity by $\sim 25\%$ (Mankoff et al., 2020; Carrivick et al.,

63 2022). An increasing frequency and risk of GLOFs (Nie et al., 2021; Zheng et al., 2021) is
64 threatening Asian population and infrastructures in the mountain ranges, such as the China-
65 Pakistan Economic Corridor (CPEC), as a flagship component of One Belt One Road
66 Initiative (Battamo et al., 2021; Li et al., 2021). The northern section of the CPEC passes
67 through Pamir, Karakoram, Hindu Kush and Himalaya mountains where droughts and
68 glacier-related hazards are frequent and severe (Hewitt, 2014; Bhambri et al., 2019; Pritchard,
69 2019), threatening local people, the existing, under-construction and planned infrastructures,
70 such as highways, hydropower plants and railways. Understanding the risk posed by water
71 shortage and glacier-related hazards is a critical step to sustainable development for the
72 CPEC.

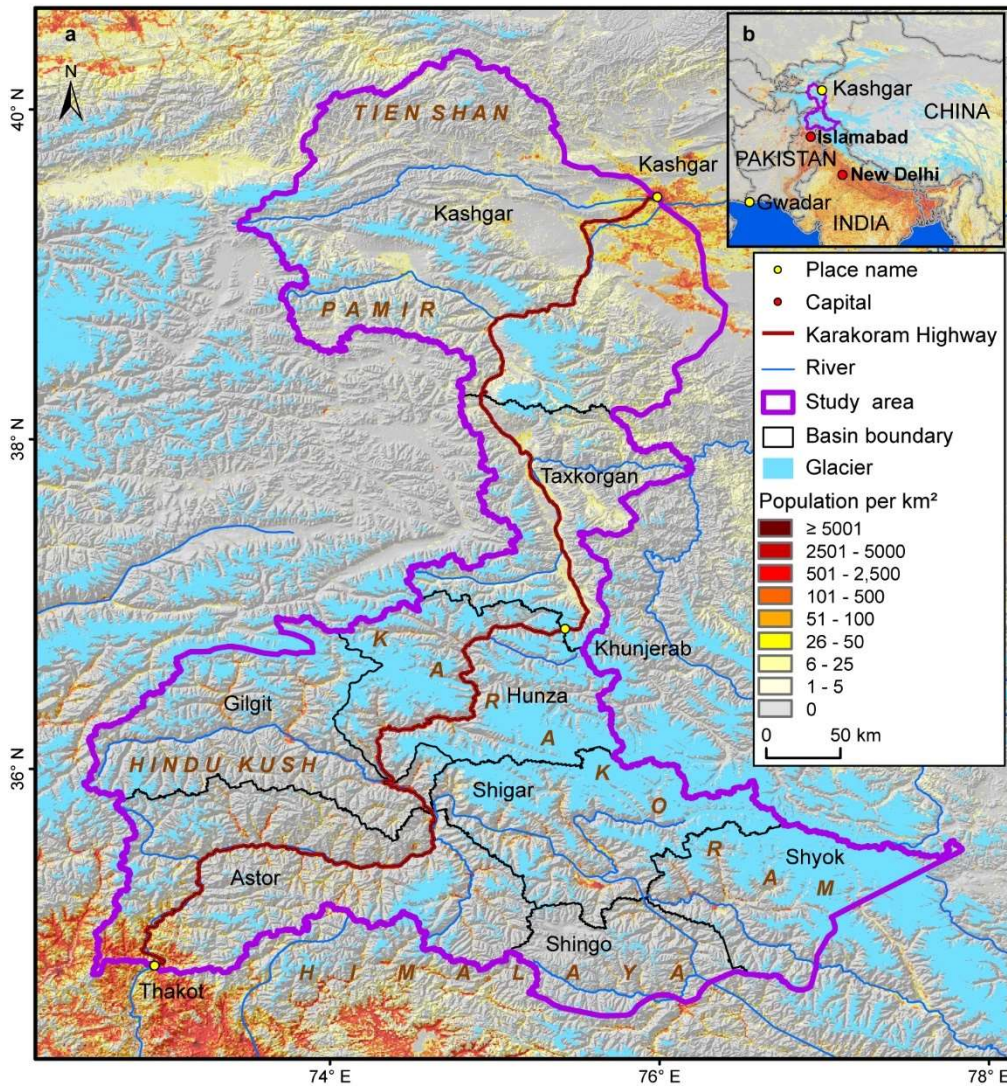
73 Glacial lake inventories with a range of attributes benefit water resource assessment and
74 disaster risk assessment related to glacial lake (Wang et al., 2020; Carrivick et al., 2022), and
75 contribute to predicting glacier-lake evolution and cryosphere-hydrosphere interactions under
76 climate change (Nie et al., 2017; Brun et al., 2019; Maurer et al., 2019; Carrivick et al., 2020;
77 Liu et al., 2020). Remote sensing is the most viable way to map glacial lakes and detect their
78 spatio-temporal changes in the high-elevation zones where in situ accessibility is extremely
79 low (Huggel et al., 2002; Quincey et al., 2007). Studies in glacial lake inventories using
80 satellite observations have been heavily conducted at regional scales recently, such as in the
81 Tibetan Plateau (Zhang et al., 2015), the Himalaya (Gardelle et al., 2011; Nie et al., 2017),
82 the HMA (Wang et al., 2020; Chen et al., 2021), the Tien Shan (Wang et al., 2013), the
83 Alaska (Rick et al., 2022), the Greenland (How et al., 2021) and the northern Pakistan
84 (Ashraf et al., 2017). However, the latest glacial lake mapping in 2020 is still absent along the
85 CPEC. Among existing studies, Landsat archival images are the most widely used due to their
86 multi-decadal record of earth surface observations, reasonably high spatial resolution (30 m),
87 and publicly available distribution (Roy et al., 2014). Freely available Sentinel-2 satellite
88 images show a better potential than Landsat in glacial lake mapping and inventories due to
89 their higher spatial resolution (10 m) and a global coverage, but have only been available
90 since late 2015 (Williamson et al., 2018; Paul et al., 2020). Glacial lake inventories using
91 Sentinel-2 images are relatively scarce at regional scales, and studies of the latest glacial lake
92 mapping as well as comparisons of glacial lake dataset derived from Sentinel-2 and Landsat
93 observations are still lacking.

94 Discrepancies between various glacial lake inventories (Zhang et al., 2015; Shugar et al.,
95 2020; Wang et al., 2020; Chen et al., 2021; How et al., 2021) result from differences in
96 mapping methods, minimum mapping units, definition of glacial lakes, time periods, data
97 sources and other factors. For example, manual vectorization method was widely adopted at
98 the earlier stage for its high accuracy. However, it is time-consuming associated with high
99 labor intensity and is only practical at regional scales (Zhang et al., 2015; Wang et al., 2020).
100 Automated and semi-automated lake mapping methods, such as multi-spectral index
101 classification (Gardelle et al., 2011; Nie et al., 2017; Zhang et al., 2018; How et al., 2021),
102 have been developed to improve the efficiency of glacial lake inventories using optical
103 images, although manual modification is often unavoidable to assure the quality of lake data
104 impacted by cloud cover, mountain shadows, seasonal snow cover and frozen lake surfaces
105 (Sheng et al., 2016; Wang et al., 2017, 2018). Backscatter images from Synthetic Aperture
106 Radar (SAR) (Wangchuk and Bolch, 2020; How et al., 2021) were used to remove the impact

107 of cloud cover for lake mapping. Besides, other approaches such as hydrological sink
108 detection using DEM (How et al., 2021) and land surface temperature-based detection
109 method (Zhao et al., 2020) were also used for lake inventories. Different classification
110 methods impact the results of lake mapping and monitoring. So far, we are lacking a unified
111 standard for the classification system of glacial lakes (Yao et al., 2018). Existing
112 classification systems are generally used for their individual research purposes, mainly based
113 on the relative positions of glacial lakes and glaciers, the supply conditions of glaciers, and
114 the attributes of dams. In addition to different classification standards, the same type of
115 glacial lakes may also have different names given by different scholars. For example, ice-
116 marginal (Carrivick and Quincey, 2014; Carrivick et al., 2020), ice-contact (Carrivick and
117 Tweed, 2013) and proglacial (Nie et al., 2017) lakes all represent glacial lakes sharing the
118 boundary with glaciers. Glacier lakes in currently available datasets have been traditionally
119 categorized by their spatial relationship with upstream glaciers (Gardelle et al., 2011; Wang
120 et al., 2020; Chen et al., 2021), and classification attributes considering the formation
121 mechanism and the properties of dams are rare or incomplete in the CPEC (Yao et al., 2018;
122 Li et al., 2020). Dam type classification of glacial lakes provides a crucial attribute for
123 glacier-lake interactions and risk assessment (Emmer and Cuřín, 2021). Therefore, an up-to-
124 date glacial lake dataset with critical, quality-assured parameters (e.g. lake area, volume and
125 type) is necessary.

126 This study aims to (1) present an up-to-date glacial lake dataset in the CPEC in 2020 using
127 both Landsat 8 and Sentinel-2 images to accurately document its detailed lake distribution;
128 (2) present two historical glacial lake datasets for the CPEC to show extent in 1990 and 2000
129 using consistent 30-m Landsat images to reveal glacial lake changes at three time periods
130 (1990, 2000 and 2020); and (3) generate a range of critical attributes for glacial lake
131 inventories to benefit studies on water resource evaluation, risk assessment of GLOFs, glacier
132 –lake evolution modeling in the HMA.

133 **2 Study area**



134
 135 **Figure 1.** Location of the study area associated with distribution of glaciers (RGI Consortium, 2017),
 136 mountains, basins and population (Rose et al., 2021) (a), and its location within the CPCE (b).
 137

138 The northern part of the CPCE is selected as the study area (Figure 1). The CPCE, originating
 139 from Kashgar of the Xinjiang Uygur Autonomous region, China and extending to Gwadar Port,
 140 Pakistan (Ullah et al., 2019; Yao et al., 2020), is connecting China and Pakistan via the only
 141 Karakoram Highway. The study area covers all the drainage basins along Karakoram Highway
 142 starting from Kashgar and ending at Thakot, with a total area of ~125,000 km². The upper Indus
 143 basins beyond the Pakistani-administrated border are excluded in this study due to spatial
 144 coverage of the CPCE. The entire study area is divided into eight sub-basins, covering most of
 145 the Karakoram with the highest elevation up to 8611 m, western Himalaya and Tien Shan,
 146 eastern Hindu Kush and Pamir Mountains. The 9710 glaciers in the study area cover a total
 147 area of 17,447 km² and nearly 60% of glaciers are distributed in the Karakoram (5818 glaciers
 148 with a total area of 14,067.52 km²) (RGI Consortium, 2017). Most glaciers in the western
 149 Himalaya and eastern Hindu Kush are losing mass in the context of climate change (Kääb et

150 al., 2012; Yao et al., 2012; Brun et al., 2017; Shean et al., 2020; Hugonnet et al., 2021), whereas
151 the glaciers in the eastern Karakoram and Pamir have shown unusually little changes, including
152 unchanged, retreated, advanced and surged glaciers (Hewitt, 2005; Kääb et al., 2012; Bolch et
153 al., 2017; Brun et al., 2017; Shean et al., 2020; Nie et al., 2021). The spatially heterogeneous
154 distribution and changes of glaciers are primarily explained as a result of differences in the
155 dominant precipitation-bearing atmospheric circulation patterns that include the winter
156 westerlies the Indian summer monsoon, their changing trends and their interactions with local
157 extreme topography (Yao et al., 2012; Azam et al., 2021; Nie et al., 2021).

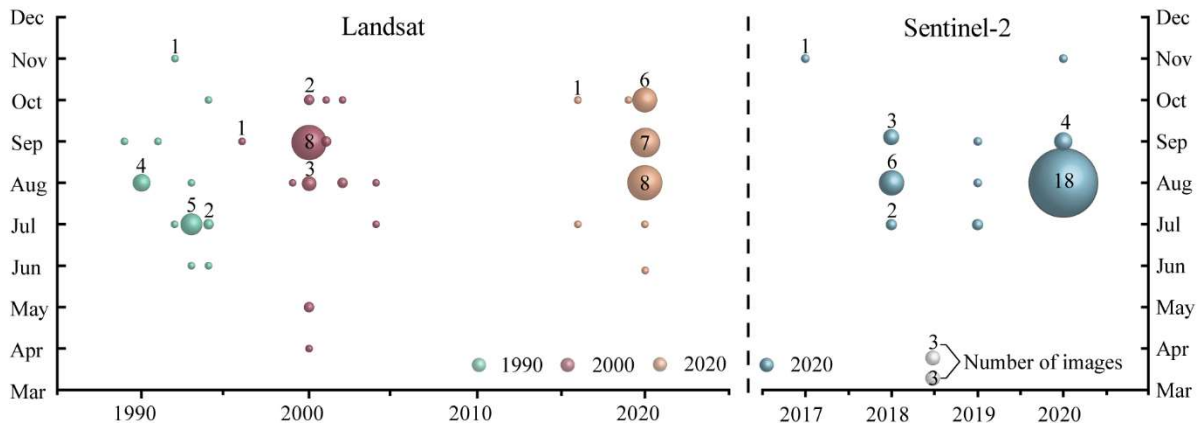
158 **3 Data sources**

159 Both Landsat and Sentinel-2 images have been employed to map glacial lakes between 1990
160 and 2020 in the CPEC (Figure 2). A total number of 71 Landsat Thematic Mapper (TM),
161 Thematic Mapper Plus (ETM+) and Landsat 8 Operational Land Imager (OLI) images with a
162 consistent spatial resolution of 30 m were downloaded from the United States Geological
163 Survey Global Visualization Viewer (GloVis, <https://glovis.usgs.gov/>) to be used to create
164 glacial lake inventories in 1990, 2000 and 2020. High-quality Landsat-5 images around 2010
165 are insufficient to cover the entire study area, so we were unable to map lakes in 2010 due to
166 Landsat-7's scan-line corrector errors and significant cloud covers. In addition, 39 Sentinel-2
167 images (23 scenes in 2020) were downloaded from Copernicus Open Access Hub
168 (<https://scihub.copernicus.eu/>) to produce the 10-m resolution glacial lake inventory in 2020.
169 All images used in this study have been orthorectified before download, but we still find that
170 one Sentinel-2 image was not well matched with Landsat images, leading to the discrepancy
171 between the two glacial lake datasets. We manually georeferenced the shifted image to
172 minimize the difference between Sentinel and Landsat derived glacial lakes.

173 Cloud and snow covers heavily affect the usability of optical satellite images (Wulder et
174 al., 2019) and their availability in the entire study area, so we took advantage of the images
175 acquired before and after each of the baseline years 1990, 2000 and 2020 to construct the
176 glacial lake inventories. Only 4 images in 1990 (the largest covering the study area), 16
177 images in 2000 and 23 images in 2020 were used for matching baseline year. Spatially, high-
178 quality images in given baseline years were preferentially chosen, or we selected one or more
179 alternative images acquired in adjacent years to delineate glacial lakes by removing the effect
180 of cloud and snow covers. To minimize the impact of intra-annual changes of glacial lakes,
181 most of used images (82% for Sentinel-2 and 75% for Landsat) were acquired from August to
182 October in the given baseline year with cloud coverage of <20% for each image. For some
183 specific scenes where cloud cover exceeded the threshold of 20%, we selected more than one
184 image to remedy the effect of cloud contamination (Nie et al., 2010, 2017; Jiang et al., 2018).

185 Other datasets used include the Randolph Glacier Inventory version 6.0 (Pfeffer et al.,
186 2014; RGI Consortium, 2017) and the Glacier Area Mapping for Discharge from the Asian
187 Mountains (GAMDAM) glacier inventory (Sakai, 2019). These two glacier datasets were
188 used to determine glacial lake types, such as ice-contact, ice-dammed and unconnected-
189 glacier-fed lakes. The Shuttle Radar Topography Mission Digital Elevation Model (SRTM
190 DEM) at a 1-arc second (30 m) resolution (Jarvis et al., 2008) was employed to extract the
191 altitudinal characteristics of the glacial lakes. The absolute vertical accuracy of the SRTM
192 DEM is 16 m (90%) (Rabus et al., 2003; Farr et al., 2007). We also applied other published

193 glacial lake datasets for comparative analysis. They include the glacial lake inventories of
 194 HMA in 1990 and 2018 downloaded from <http://doi.org/10.12072/casnw.064.2019.db> (Wang
 195 et al., 2020), the Third Pole region in 1990, 2000 and 2010 publicly shared at
 196 <http://en.tpdatabase.cn/> (Zhang et al., 2015), the Tibet Plateau from 2008 to 2017 accessed at
 197 <https://doi.org/10.5281/zenodo.3700282> (Chen et al., 2021), and the entire world in 1990,
 198 2000 and 2015 provided at https://nsidc.org/data/HMA_GLI/versions/1 (Shugar et al.,
 199 2020). In addition, field survey data collected between 2017 and 2018 were also used to assist
 200 in lake mapping and glacial lake type classification.
 201

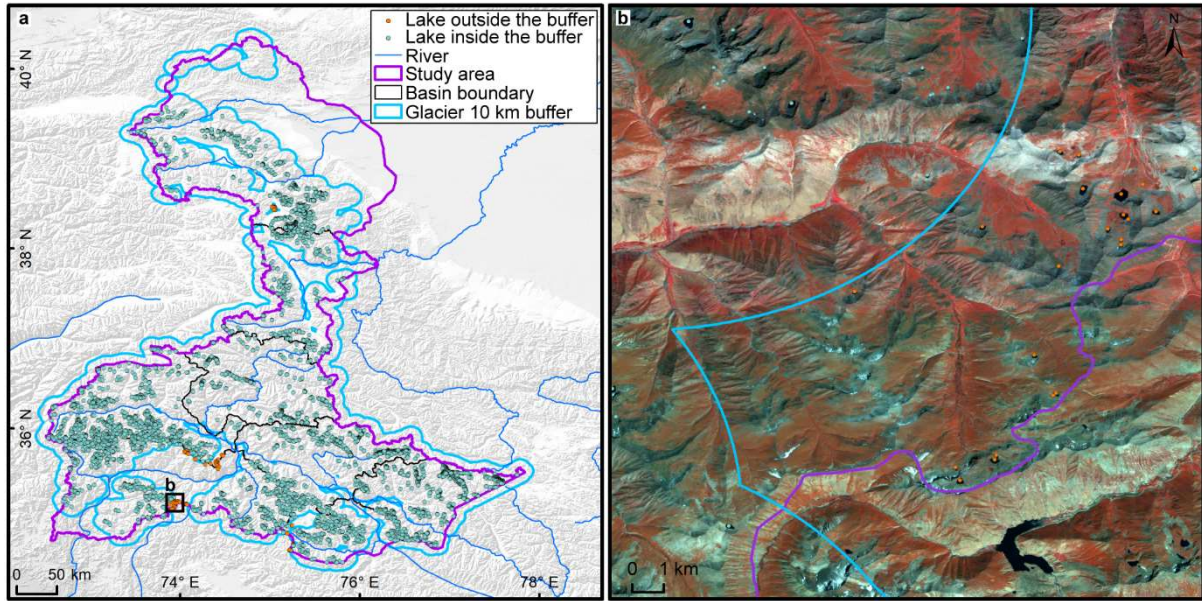


202
 203 **Figure 2.** Acquisition years and months of Landsat and Sentinel-2 images selected for glacial lake
 204 inventories. The bubble size indicates the available high-quality image number.

205 4 Glacial lake inventory methods

206 4.1 Definition of glacial lakes

207 We consider a glacial lake as one that formed as a result of modern or ancient glaciation.
 208 Contemporary glacial lakes are easily recognized using a combination of glacier inventories
 209 and remote sensing images. Ancient glacial lakes can be identified from periglacial
 210 geomorphological characteristics, including moraine remnants and U-shaped valleys that are
 211 discernible from satellite observations (Post and Mayo, 1971; Westoby et al., 2014; Nie et al.,
 212 2018; Martín et al., 2021). A 10-km buffering distance of RGI 6.0 glacier boundaries that has
 213 been widely used in previous studies (Zhang et al., 2015; Wang et al., 2020), was created to
 214 help mapping glacial lakes. A few glacial lakes in the study area (a total of 84 lakes for
 215 Sentinel-2 dataset and 55 lakes for Landsat dataset in 2020) beyond the buffering zone,
 216 located near buffering boundaries, were intentionally included due to clear evidence of
 217 glaciation (**Figure 3**). Landslide-dammed lakes (Chen et al., 2017) in the buffering zone were
 218 excluded in our inventories because of their irrelevance to glaciation. All glacial lakes in the
 219 study area were mapped according to our definition. We were able to implement this
 220 definition by carefully leveraging the spectral properties of glacial lakes and the periglacial
 221 geomorphological features that are often evident in remote sensing images (see more in
 222 sections 4.3 and 4.4).
 223



224
225
226
227

Figure 3. The 10-km buffer zone of RGI 6.0 glacier boundaries (a) and Sentinel-derived glacial lakes located near buffering boundary within the study area (b).

228 4.2 Interactive lake mapping

229 A human-interactive and semi-automated lake mapping method (Wang et al., 2014; Nie et al.,
230 2017, 2020) was adopted to accurately extract glacial lake extents using Landsat and
231 Sentinel-2 images, based on the Normalized Difference Water Index (NDWI) (Mcfeeters,
232 1996). The NDWI uses the green and near infrared bands and is calculated by the following
233 equation:

$$234 \quad NDWI = \frac{Band_{Green} - Band_{NIR}}{Band_{Green} + Band_{NIR}} \quad (1)$$

235 where the green band and near infrared band were provided by both Landsat and Sentinel
236 multispectral images.

237 Specifically, the method calculated the NDWI histogram based on the pixels with each
238 user-defined and manually-drawn region of interest. The NDWI threshold that separates lake
239 surface from land was interactively determined by screening the NDWI histogram against the
240 lake region in the imagery (Wang et al., 2014; Nie et al., 2020). This way, the determined
241 NDWI threshold can be well-tuned to adapt various spectral conditions of the studied glacier
242 lakes. The raster lake extents segmented by the thresholds were then automatically converted
243 to vector polygons. We first completed the glacial lake inventory in 2020 using this
244 interactive mapping method, and the 2020 inventory was then used as a reference to facilitate
245 the lake mapping for other periods.

246 The minimum mapping unit (MMU) was set to 5 pixels for both Landsat (0.0045 km²) and
247 Sentinel-2 images (0.0005 km²) in this study. MMU determines the total number and area of
248 glacial lakes in the dataset, and varies in the previous studies, such as 3 pixels (Zhang et al.,
249 2015), 6 pixels (Wang et al., 2020), or 9 pixels (Chen et al., 2021) for a regional scale, or 55
250 pixels (Shugar et al., 2020) for a global scale. While a smaller threshold leads to a large
251 quantity of lakes mapped, it also generates larger mapping noises or uncertainties.

252 Considering this signal-noise balance and our focus on identifying prominent glacier lake
253 dynamics in the study area, we opted to use 5 pixels as the MMU for both Landsat and
254 Sentinel-2 images.

255 Several procedures were taken to assure the quality assurance and quality control for lake
256 mapping, including 1) visual inspection and modification using the threshold-based mapping
257 method for each lake according to Landsat, Sentinel-2 and Google Earth high-resolution
258 images overlaying preliminarily lake boundary extraction at the given time period; 2) time
259 series check for Landsat-derived glacial lake datasets from 1990 and 2020, and cross-check
260 between Landsat and Sentinel-2-derived lake dataset in 2020 to reduce errors of omission and
261 commission; 3) topological validation of glacial lake mapping, such as repeated removal,
262 elimination of small sliver polygons; and 4) logical check for lake types between two
263 classification systems of glacial lakes. False lake extents resulting from cloud or snow cover,
264 lake ice, and topographic shadows (Nie et al., 2017, 2020) were modified using previous
265 semi-automated mapping method based on alternative images acquired in adjacent years.
266 Those procedures were time-consuming, but helped to minimize the effect of cloud and snow
267 covers, lake mapping errors, and to maximize the quality of the produced lake product and
268 the derived glacial lake changes.

269 4.3 Classification of glacial lakes

270 Two glacial lake classification systems (GLCS) have been established based on relationship
271 of interaction between glacial lakes and glaciers as well as lake formation mechanism and
272 dam material properties. In the first GLCS (GLCS1), glacial lakes were classified into four
273 types based on their spatial relationship to upstream glaciers: supraglacial, ice-contact,
274 unconnected-glacier-fed lakes, and non-glacier-fed lakes according to Gardelle et al. (2011)
275 and Carrivick et al. (2013). Alternatively, combining the formation mechanism of glacial
276 lakes and the properties of natural dam features, glacial lakes were classified into five
277 categories (herein named GLCS2) modified from Yao's classification system (2018):
278 supraglacial, end-moraine-dammed, lateral-moraine-dammed, glacial-erosion lakes and ice-
279 dammed lakes. Subglacial lakes were excluded due to the mapping challenge from spectral
280 satellite images alone. Characterization and examples for each type are provided in Table 1
281 and Table 2. Individual glacial lakes were categorized to the specific types for each GLCS
282 according to available glacier inventory data, geomorphological and spectral characteristics
283 interpreted from Landsat, Sentinel and Google Earth images. The synergy of these two
284 GLCSs is beneficial to predicting glacier-lake evolutions and providing fundamental data for
285 water resource and glacial lake disaster risk assessment.

286

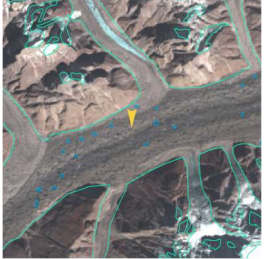


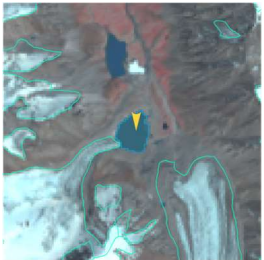
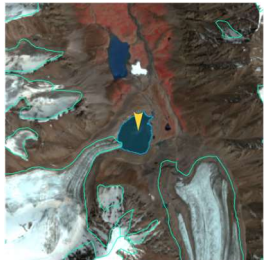
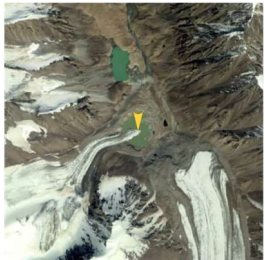
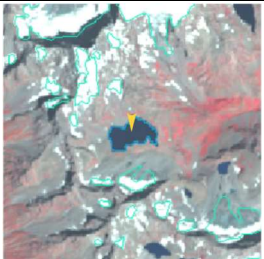
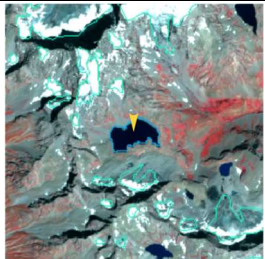
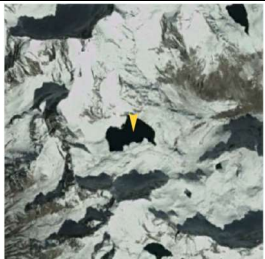

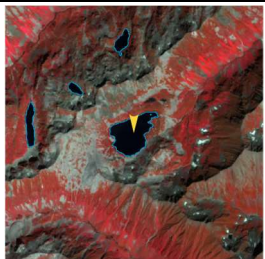
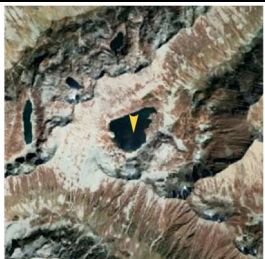
287

288

289




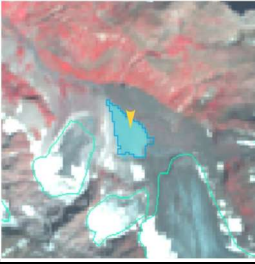
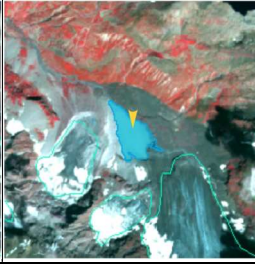








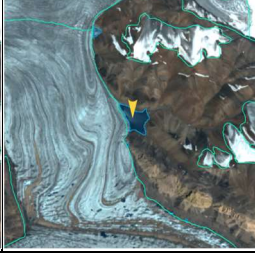
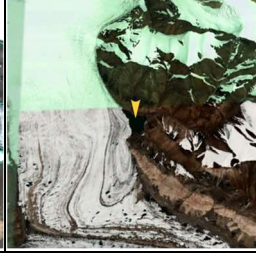
290

Table 1. Classification system of glacial lake types according to the relationship between glacial lakes and glaciers (© Google Earth 2019). Glacier outlines are from RGI 6.0 (RGI Consortium, 2017), and the yellow marker represents target lake.

Lake types	Characteristics	Landsat	Sentinel-2	Google Earth
Supraglacial	Lakes formed on the surface of glaciers, generally dammed by ice and thin debris. Case location: 35°43'49.74" N 76°13'53.88" E			
Ice-contact	Lakes dammed by moraine, ice or bedrock, supplied by glacial meltwater and shared boundary with glaciers. Case location: 39°09'32.40" N 73°43'12.00" E			
Unconnected-glacier-fed	Lakes currently supplied by upstream glacial meltwater but disconnected with glaciers. Case location: 35°47'60.00" N 72°55'15.60" E			
Non-glacier-fed	Lakes formed by glaciology, dammed by moraine or bed rock, and currently not supplied by glacial meltwater. Case location: 34°50'39.99" N 74°48'29.31" E			

291

292 **Table 2.** Classification system of glacial lake types according to the formation mechanism of glacial lakes
 293 and dam material properties (© Google Earth 2019). Glacier outlines from RGI 6.0 (RGI Consortium,
 294 2017), and the yellow marker represents target lake.

Lake types	Characteristics	Landsat	Sentinel-2	Google Earth
Supraglacial	Lakes formed on the surface of glaciers, generally dammed by ice and thin debris. Case location: 36°46'7.39" N 74°20'7.59" E			
End-moraine-dammed	Lakes formed behind moraines as a result of glacier retreat and downwasting. Case location: 35°42'50.40" N 73°09'57.60" E			
Lateral-moraine-dammed	Lakes formed behind lateral glacial moraine ridges and dammed by debris, different from ice-dammed glacial lake. Case location: 38°28'45.62" N 75°20'52.30" E			
Glacial-erosion	Lakes formed in depressions created by glacial over-deepening. Bedrock dam dominates, partially superimposed by top moraine in rugged terrain. Dams are unclear in the satellite images. Case location: 35°55'55.56" N 73°38'20.13" E			
Ice-dammed	Lakes formed behind glaciers, dammed by glacier ices (partially covered by debris on the top). Case location: 35°28'31.32" N 77°30'46.81" E			

295

296 4.4 Attributes of glacial lake data

297 A total of 18 attribute fields were input into our glacial lake datasets (Table 3). They include
 298 lake location (longitude and latitude), lake elevation (centroid elevation), orbital number of the
 299 image source, image acquisition date, lake area, lake perimeter, lake types of the two GLCSs,
 300 mapping uncertainty, lake water volume and the country, sub-basin, and mountain range
 301 associated with the lake. Amongst the attributes, lake location was calculated based on the

302 centroid of each glacial lake polygon associated with the DEM, N represents northing and E
 303 represents easting. Orbital number of the image source was filled with the corresponding
 304 satellite image, with the codes expressed as “PxxxRxxx” or “Txxxxx”, where P and R indicate
 305 the path and row for Landsat image and T represents the tile of Sentinel-2 image associated
 306 with 5 digit code of military grid reference system. Area and perimeter were automatically
 307 calculated based on glacial lake extents. Lake water volume was estimated by area-volume
 308 empirical equation (Cook and Quincey, 2015). Lake types were attributed using the
 309 characterization and interpretation marks described in Section 4.3. Mapping uncertainty was
 310 estimated using our modified equation which will be introduced in section 4.5 and appendix
 311 tutorial. Located country, sub-basin and mountain range of each glacial lake was identified by
 312 overlapping the geographic boundaries of countries, basins and mountain ranges.

313
 314 **Table 3.** Attributes of glacial lake dataset.

Field Name	Type	Description	Note
FID or OBJECTID	Object ID	Unique code of glacial lake	Number
Shape	Geometry	Feature type of glacial lake	Polygon
Latitude	String	Latitude of the centroid of glacial lake polygon	Degree minute second
Longitude	String	Longitude of the centroid of glacial lake polygon	Degree minute second
Elevation	Double	Elevation of the centroid of glacial lake polygon	Unit: meter above sea level
IMGSOURCE	String	Path and row numbers for Landsat image based on World Reference System 2 or Tile number for Sentinel image based on military grid reference system	PxxxRxxx or Txxxxx
ACQDATE	String	Acquisition date of source image	YYYYMMDD
GLCS1	String	The first classification system of glacial lakes based on relationship of interaction between glacial lakes and glaciers	Supraglacial, Ice-contact, Unconnected-glacier-fed, None-glacier-fed
GLCS2	String	The second classification system of glacial lakes based on lake formation mechanism	Supraglacial, End- moraine-dammed, Lateral-

Field Name	Type	Description	Note
		and dam material properties	moraine-dammed, Glacial-erosion and Ice-dammed
Basin	String	Basin name where glacial lake locates in	
Mountain	String	Mountain name where glacial lake locates in	
Country	String	Country name where glacial lake locates in	
Perimeter	Double	Perimeter of glacial lake boundary	Unit: meter
Area	Double	Area of glacial lake coverage	Unit: square meter
Uncertainty	Double	Uncertainty of glacial lake mapping estimated based on modified Hanshaw's equation (2014)	Unit: square meter
Volume	Double	Water volume of glacial lake estimated by area-volume empirical equation	Unit: square meter
Operator	String	Operator of glacial lake dataset	Muchu, Lesi
Examiner	String	Examiner of glacial lake dataset	Yong, Nie

315

316 4.5 Error and uncertainty assessment

317 4.5.1 Improved uncertainty estimating method

318 We modified Hanshaw's (2014) equation that had been used to calculate lake-area mapping
319 uncertainty. Lake perimeter and displacement error are widely used to estimate the
320 uncertainty of glacier and lake mapping from satellite observation (Carrivick and Quincey,
321 2014; Hanshaw and Bookhagen, 2014; Wang et al., 2020). Hanshaw and Bookhagen (2014)
322 proposed an equation to calculate the error of area measurement by the number of edge pixels
323 of the lake boundary multiplied by half of a single pixel area. The number of edge pixels is
324 simply calculated by the perimeter divided by the grid size. The equation is expressed as
325 below:

$$326 \quad Error(1\sigma) = \frac{P}{G} \times 0.6872 \times \frac{G^2}{2} \quad (2)$$

$$327 \quad D = \frac{Error(1\sigma)}{A} \times 100\% \quad (3)$$

328 Where G is the cell size of the remote sensing imagery (10 m for Sentinel-2 image and 30 m
329 for Landsat image). P is the perimeter of individual glacial lake (m), and the coefficient of
330 0.6872 (1σ), which means nearly 69% of the edge pixels are subject to errors (Hanshaw and

331 Bookhagen, 2014), was chosen assuming that area measurement errors follow a Gaussian
 332 distribution. Relative error (D) was calculated by equation 3, in which A is the area of an
 333 individual glacial lake.

334 In the original equation 2, the number of edge pixels varies by the shape of lake and is
 335 indicated by $\frac{P}{G}$. However, the pixels in the corner are double counted (Figure 4). The total
 336 number of repeatedly calculated edge pixels equals the number of inner nodes. Therefore, we
 337 adjusted the calculation of the actual number of edge pixels as the maximum of edge pixels
 338 ($\frac{P}{G}$) subtracting the number of inner nodes. Accordingly, the equation of uncertainty
 339 estimation for lake mapping is modified as below:

$$340 \quad Error(1\sigma) = \left(\frac{P}{G} - N_{Inner} \right) \times 0.6872 \times \frac{G^2}{2} \quad (4)$$

341 Where N_{Inner} is the number of inner nodes (inflection points) of each lake. The modified
 342 equation is also suitable for lakes with islands (as illustrated in Figure 4b).

343 For polygons without islands (Figure 4a), use the following equation:

$$344 \quad N_{Inner} = \left(\frac{N_{Total} - 4 - 1}{2} \right) \quad (5)$$

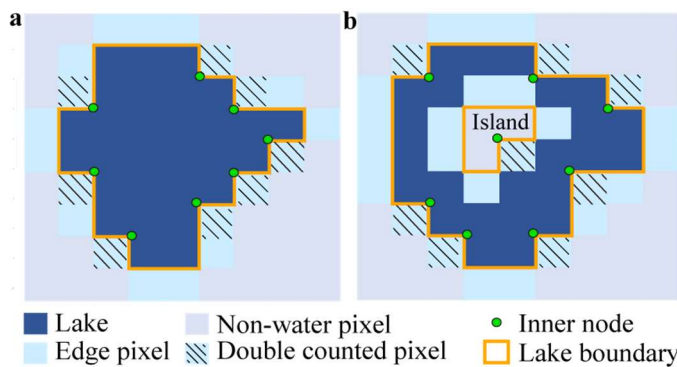
345 N_{Total} is the total number of nodes, including both the outer and inner. N_{Total} is calculated
 346 by the “Field Calculator” in ArcGIS, in some cases, it is necessary to remove the redundant
 347 nodes before calculating the total number of nodes (See the Appendix for more details). An
 348 inner node is a polygon vertex where the interior angle surrounding it is greater than 180
 349 degrees. An outer node is the opposite of the inner node, where the interior angle is less than
 350 180 degrees. We found that the outer nodes are usually four more than the inner nodes in our
 351 glacial lake dataset. The total nodes in ArcGIS contain one overlapping node to close the
 352 polygon, meaning the endpoint is also the startpoint. This extra count was deleted in the
 353 calculation (equation 5).

354 For polygons with island (Figure 4b) use the following equation:

$$355 \quad N_{Inner} = \left(\frac{N_{Total} - (N_{Island} + 1) \times 5}{2} \right) \quad (6)$$

356 N_{Island} is the number of islands within each polygon. A calculation method of N_{Island} is
 357 given in the Appendix.

358



359

360 **Figure 4.** Sketch of estimating the actual edge pixels for uncertainty calculation of individual glacial lake
 361 (with (a) and without islands (b)).

362

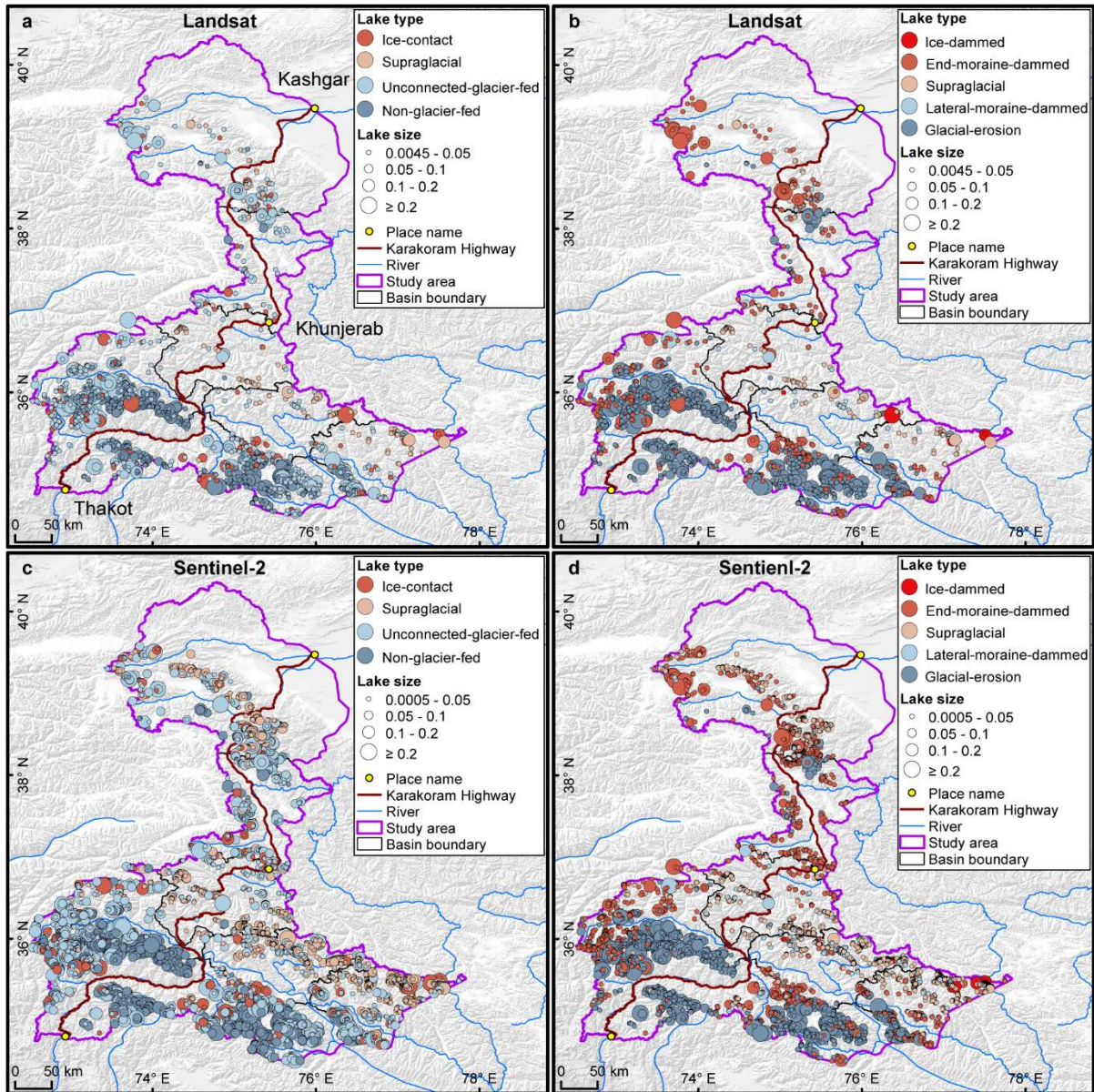
363 4.5.2 Validation of glacial lake mapping

364 A total of 89 glacial lakes were selected by stratified random sampling and manually digitized
365 based on the Google Earth high resolution images to further validate the absolute error of the
366 glacial lake mapping in 2020 due to lacking of field measurements for glacial lakes in the
367 study area. During the sampling, we set a regulation of minimum lake area greater than 4500
368 m² and relative differing between Landsat- and Sentinel-derived lake areas less than 18%
369 (nearly equaling to the average relative error of $\pm 17.36\%$ for Landsat lake mapping) to
370 minimize the effect of lake changes from multi-temporal satellite observations in circa 2020.
371 The 89 sample lakes range from 0.005 km² to 0.802 km² with a median (standard deviation)
372 size of 0.047 ± 0.134 km² and total area of 8.033 km² for Landsat-derived dataset, whereas
373 ranging from 0.005 km² to 0.849 km² with a median (standard deviation) size of 0.045 ± 0.144
374 km² and total area of 8.447 km² for Sentinel-derived dataset.
375

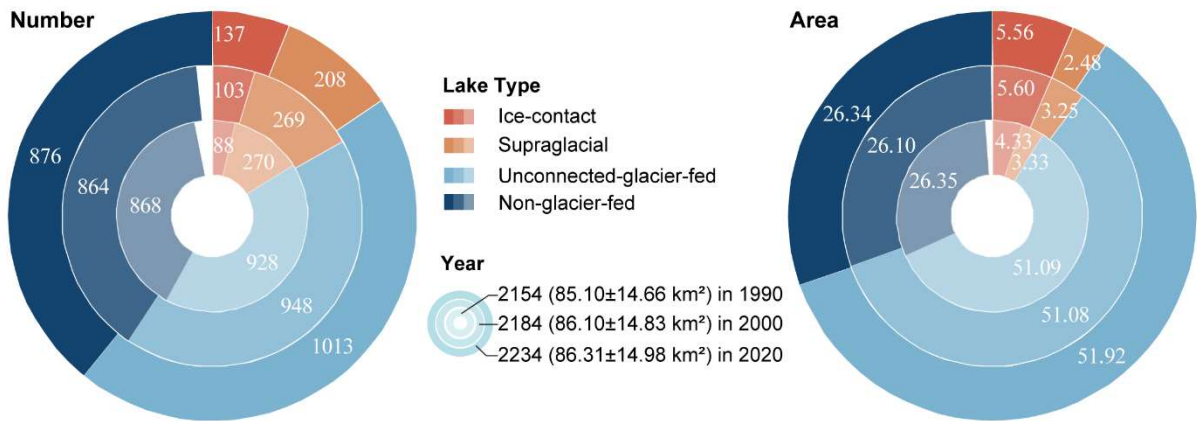
376 5 Results

377 5.1 Glacier lake distribution and changes observed from Landsat

378 We mapped 2,234 glacial lakes for 2020 across the studied CPEC from Landsat-8 images,
379 with a total area of 86.31 ± 14.98 km² (Figure 5a and b). Unconnected-glacier-fed lakes are
380 dominant in the first classification system, followed by non-glacier-fed lakes (Figure 6)
381 whereas glacial-erosion lakes dominate at both number (1478) and area (57.02 km²) in the
382 second classification system (Figure 7), followed by end-moraine-dammed lakes and
383 supraglacial lakes. Among the classified lakes, 137 are ice-contact lakes and cover an area of
384 5.56 km², implying a higher mean size of ice-contact lakes than supraglacial lakes.
385

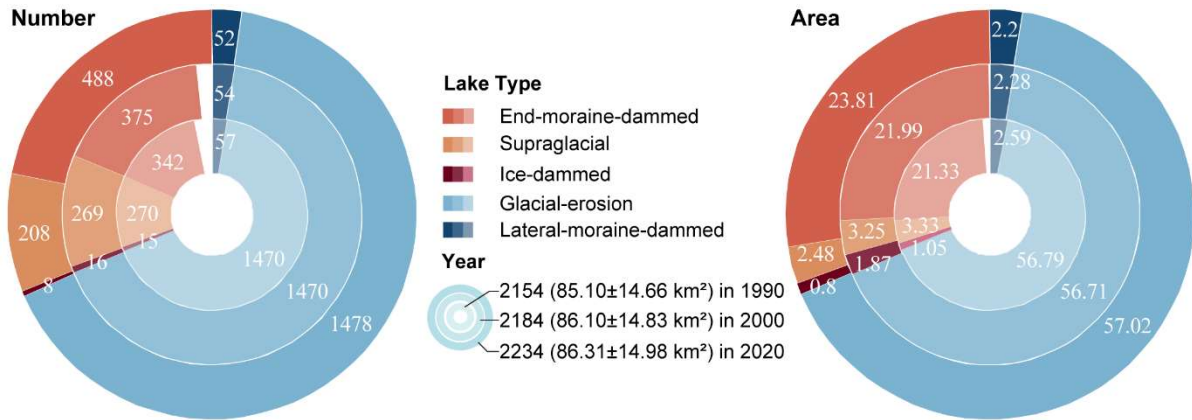


386
 387 **Figure 5.** Distribution of glacial lakes in 2020 extracted from Landsat (a, b) and Sentinel-2 (c, d) images.
 388 Panels a and c are classified by GLCS1, and GLCS2 for sub-graph b and d.
 389



390
 391 **Figure 6.** Number and area of different types of glacial lakes classified based on the condition of glacier

392 supply in the study area (GLCS 1). The outermost ring represents glacial lake data in 2020, middle ring for
 393 2000 and innermost ring for 1990. Lake number and area in 2020 were selected as reference, meaning a
 394 concept of "100 %" for a complete ring. Labeled values are scaled in degrees rather the radius of rings.
 395



396
 397 **Figure 7.** Number and area of different types of glacial lakes classified based on glaciation and nature of
 398 dam in the study area (GLCS 2). The outermost ring represents glacial lake data in 2020, middle ring for
 399 2000 and innermost ring for 1990. Lake number and area in 2020 were selected as reference, meaning a
 400 concept of "100 %" for a complete ring. Labeled values are scaled in degrees rather the radius of rings.
 401

402 The total number and area of glacial lakes in the study remain relatively stable with a
 403 slight increase between 1990 and 2020, and the changes in count and area among various
 404 types of glacial lakes vary substantially (Figure 6 and Figure 7). From 1990 to 2020, the total
 405 number of glacial lakes increased by 80 or 3.70%, while the area grew by 1.21 km² (or
 406 1.42%). In GLCS1, unconnected-glacier-fed lakes have the largest increase in number,
 407 followed by ice-contact and non-glacier-fed lakes, whereas supraglacial lakes decreased by
 408 62 in count. Ice-contact lakes expanded by 1.24 km² (equaling an increase of 26% in ice-
 409 contact lakes), contributed one third of the total area increase. Supraglacial lakes decreased
 410 by 0.85 km² in area whereas the areas of unconnected-glacier-fed and non-glacier-fed lakes
 411 remained stable as a result of disconnections from glaciers (Figure 6). In GLCS2, end-
 412 moraine-dammed lakes increased by 2.48 km² and contributed most of the glacier lake area
 413 expansion, whereas supraglacial, ice-dammed and lateral-moraine-dammed lakes decreased
 414 slightly in both number and area. Glacial-erosion lakes accounted for the maximum
 415 percentage (about 66% for both count and area) in each time period and remained stable
 416 (Figure 7).

417 5.2 Glacier lake distribution observed from Sentinel-2

418 Sentinel-derived results shows that there are 7,560 glacial lakes (103.70±8.45 km²) in 2020
 419 across the entire CPEC (Table 4) under a MMU of 5 pixels (500 m²). Compared with
 420 Landsat-derived product, glacial lakes from Sentinel-2 have similar spatial distribution
 421 characteristics (Figure 5); meanwhile, a larger quantity of glacier lakes, with more accurate
 422 boundaries and a greater total lake area, were generated from Sentinel-2 images. The smallest
 423 size class (0.0005-0.0045 km²) contains the maximum lake number (4,969) but the least lake
 424 area (7.73±2.62 km²) (Table 4), which is not available in the Landsat-derived lake data due to

425 a coarser spatial resolution. In each size class, there are also a higher number of larger glacial
 426 lakes from Sentinel than that from Landsat images. The discrepancy is mainly attributed to
 427 the inconsistency of spatial resolutions and image acquisition dates.

428

429 **Table 4.** Count and area of glacial lakes mapped from Sentinel-2 and Landsat images in 2020 between
 430 various size classes.

Lake size km ²	Glacial lakes from Sentinel-2 count (km ²)	Glacial lakes from Landsat count (km ²)	Overlap % (%)
0.0005-0.0045	4969 (7.73±2.62)	—	—
0.0045-0.05	2182 (35.52±3.72)	1870 (31.47±9.57)	85.70 (88.60)
0.05-0.1	237 (16.37±0.89)	204 (14.07±2.18)	86.08 (85.95)
0.1-0.2	122 (16.88±0.68)	115 (15.91±1.83)	94.26 (94.25)
≥0.2	50 (27.20±0.54)	45 (24.86±1.40)	90.00 (91.40)
Total	7560 (103.70±8.45)	2234 (86.31±14.98)	—

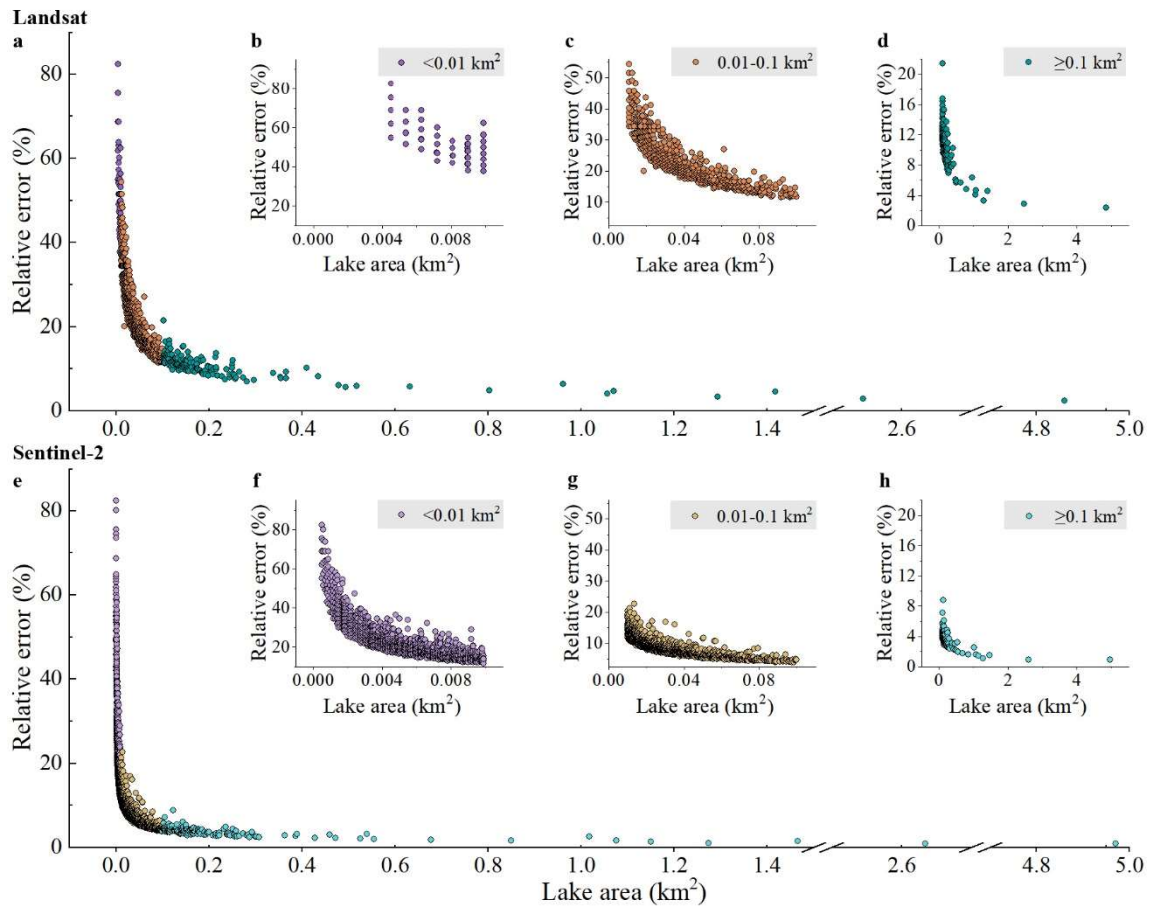
431 **Note:** Overlap % (%) represent the rates in count and area calculated by dividing Landsat-derived lake data by Sentinel-
 432 derived data in the same size class respectively.

433 6 Discussions

434 6.1 Error and uncertainty of lake mapping

435 The uncertainty estimated from our improved equation shows that the relative error of
 436 individual glacial lake decreases when lake size increases or cell size of remote sensing
 437 images reduces (Lyons et al., 2013; Carrivick and Quincey, 2014) (Figure 8). Total area error
 438 of glacial lakes in study area is approximate ±14.98 km² and ±8.45 km² in 2020 for Landsat
 439 and Sentinel-2 dataset, respectively, and the average relative error is ±17.36% and ±8.15%.
 440 Generally, small lakes have greater relative errors. For example, the mean relative error is
 441 35.38% for Landsat derived glacial lakes between 0.0045 and 0.1 km² and 10.63% for glacial
 442 lakes greater than 0.1 km². The mean area error of Sentinel-derived glacial lakes is almost
 443 one third of that extracted from Landsat images for glacial lakes of all or specific size group.
 444 Because the relative error was estimated as a function of satellite image spatial resolution and
 445 lake perimeter, the calculated error for large lake is proportionally smaller than that of small
 446 lake (Salerno et al., 2012) and the error for Landsat-derived lake is naturally greater than that
 447 of Sentinel-derived lake at the same size group.

448



449

450

Figure 8. Estimated relative error for glacial lakes of all or specific size ranges in study area. Error estimation is based on the modified equation and lake data extracted from Landsat (a-d) and Sentinel-2 images (e-h).

452

453

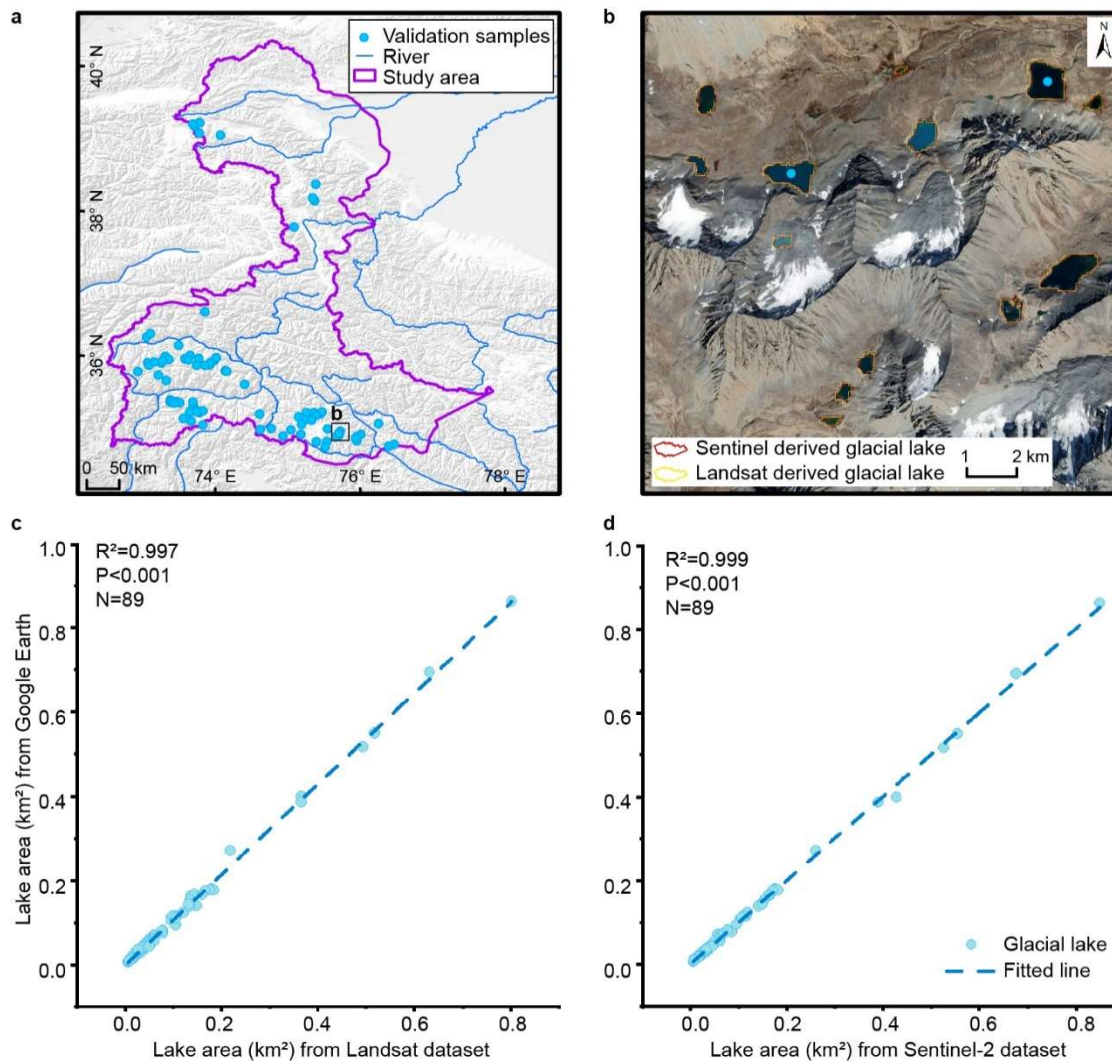
454

Our Landsat- and Sentinel-derived glacial lake dataset match well lake boundaries in Google Earth high resolution images (Figure 9). A dense cluster of validation samples along the 1:1 line indicates a high accuracy in lake mapping (Figure 9c and d). The error of 89 sample lakes is 5.48% in total area between Landsat- and Google Earth-derived data, whereas 0.61% for Sentinel- and Google Earth-derived data. The median (\pm standard deviation) in discrepancy of individual lake area is $7.66\pm 4.96\%$ for Landsat- and Google Earth-derived data, whereas $4.46\pm 4.62\%$ for Sentinel- and Google Earth-derived data. Our glacial lake dataset shows a satisfactory mapping accuracy, and of which Sentinel-derived lake data performs more accurate than those from Landsat images.

461

462

463

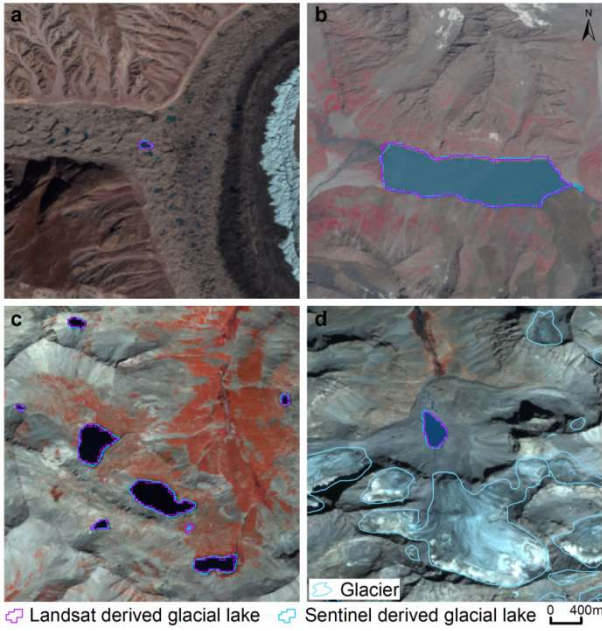


464

465 **Figure 9.** Distribution of validation samples (a), comparison of glacial lakes derived from Landsat and
 466 Sentinel-2 overlaying Google Earth image (© Google Earth 2019) in a zoomed site (b), and glacial lake
 467 product validated by Google Earth derived lake boundaries (c and d).

468 **6.2 Comparison of Sentinel-2 and Landsat derived products**

469 Glacial lakes from Landsat and Sentinel-2 images have a high consistency in number and
 470 area with overlap rates from approximately 86% to 94% for all lakes greater than 0.0045 km²
 471 (Table 4), indicating a good potential for coordinated utility with Landsat archived
 472 observation (Figure 10). Lake extents extracted from Landsat and Sentinel images match well
 473 for various types and sizes (Figure 10 and Figure 11, Table 4). The best consistency rate
 474 reaches 94% for the glacial lakes between 0.1 km² and 0.2 km². The difference in area of
 475 glacial lakes extracted from Landsat and Sentinel-2 images generally lies within the
 476 uncertainty ranges.



477

478

479

480

481

482

483

484

485

486

487

488

489

490

491

492

493

494

495

496

497

498

499

500

501

502

503

504

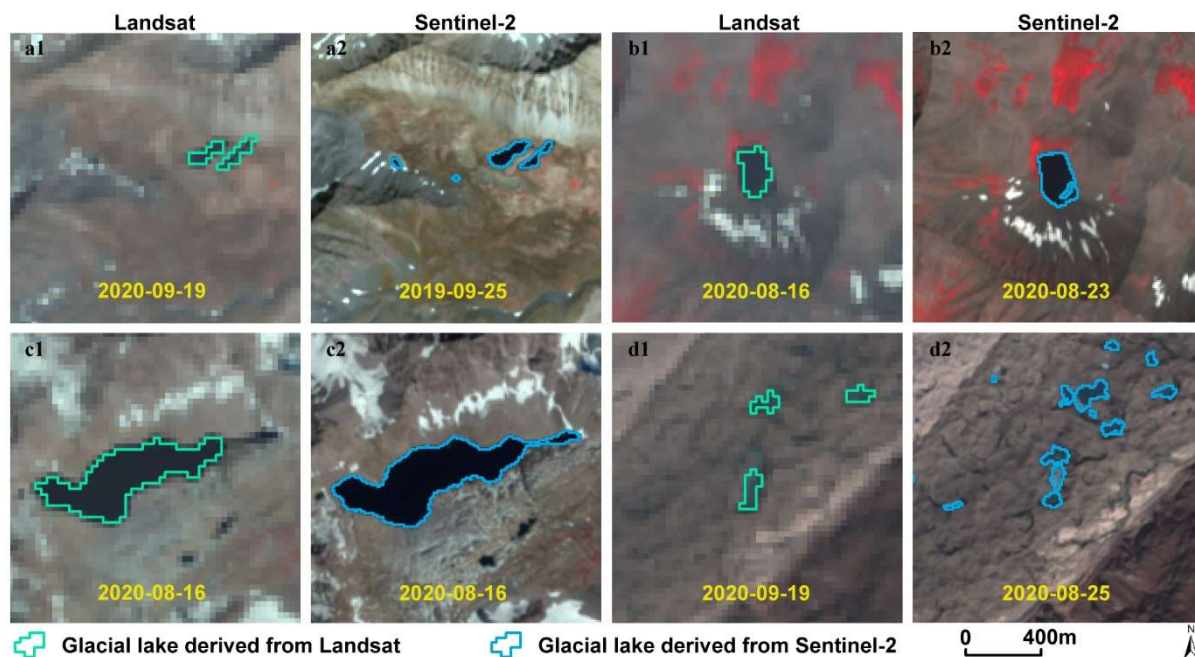
505

Figure 10. High consistency of lake extents extracted from Landsat and Sentinel-2 images. Lake types shown include supraglacial (a), glacier-fed moraine-dammed (b), unconnected glacial-erosion lake without glacier melt supply (c) and glacier-fed moraine-dammed lakes (d).

Spatial resolution of satellite images plays a primary role in the discrepancies in count and area of glacial lakes extracted from Landsat (30 m) and Sentinel-2 (10 m) observations. Due to a finer spatial resolution, Sentinel-2 images can extract more glacial lakes and more accurate extents than those from Landsat images. We set the same 5 pixels as the MMU for both Landsat and Sentinel-2 images, which corresponds to a minimum area of 0.0045 km² and 0.0005 km², respectively. The minimum mapping area results in generating nearly 5000 more lakes from Sentinel-2 images than from Landsat images, causing the greatest discrepancy in number (Table 4), such as Figure 11a. Small lakes such as supraglacial lakes play an important role in analyzing glacier evolution and supraglacial drainage systems (Liu and Mayer, 2015; Miles et al., 2018), implying a potential of our dataset to be applied in studies of glacier-lake evolutions. Meanwhile, Sentinel-2 images are able to depict boundaries of glacial lake with a lower uncertainty, as for some small islands and narrow channels (Figure 11b and c) were mapped from Sentinel-2 imagery that were unable to be detected in Landsat imagery.

Different acquisition dates between Sentinel-2 and Landsat images also contribute to the discrepancy of those two glacial lake data. Acquiring same-day images from the two sensors were not always possible due to the impacts of cloud contaminations, topographic shadows, snow cover and revisit periods (Williamson et al., 2018; Paul et al., 2020). Glacial lakes are changing temporally in the context of climate and glacier changes, taking supraglacial lakes for example that evolve dramatically in a short period observed between Landsat and Sentinel-2 images (Figure 11d). Despite our efforts of leveraging all available high-quality images, the overlap of acquisition dates between Landsat and Sentinel-2 images for the same location is relatively low (only 7 scenes of Sentinel-2 images or 112 glacial lakes in 2020) in this study area, and the consequential temporal gaps led to a difference in the number and

506 area of the derived glacial lakes.
507



508
509 **Figure 11.** Discrepancy of lake extents extracted from Landsat and Sentinel-2 images.
510

511 6.3 Limitation and updating plan

512 We would like to acknowledge several limitations of our glacier lake dataset, largely due the
513 availability of high quality satellite images in the study area and inadequate field survey data
514 (Wang et al., 2020; Chen et al., 2021). First, it is unlikely to collect enough good-quality
515 images within one calendar year for the entire study area due to high possibility of cloud or
516 snow covers. Even though the capacity of repeat observations for Landsat-8 OLI and
517 Sentinel-2 increased (Roy et al., 2014; Williamson et al., 2018; Wulder et al., 2019; Paul et
518 al., 2020), the 2020 glacial lake dataset has to employ images acquired in adjacent years
519 besides 2020. Most images used from Landsat and Sentinel-2 platforms were imaged in
520 autumn, and some images taken between April and July and in November also were
521 employed. Distribution and changes in glacial lakes primarily represent the characteristics
522 between August and October. Glacial lakes evolve with time and space (Nie et al., 2017), and
523 subtle inter- and intra-annual changes (Liu et al., 2020) for each time period were ignored.
524 Second, field investigation data are limited due to low accessibility of high mountain
525 environment in the study area, which restrained the accuracy in classifying the glacial lake
526 types. Although very high-resolution Google Earth images were utilized to assist in lake type
527 interpretation, occasional misclassification was unavoidable. We implemented two types of
528 classification systems based on a careful utilization of glacier data, DEM, geomorphological
529 features and expert knowledge. However, the lack of in situ survey prohibited a thorough
530 validation of the glacial lake types. Third, the rigorous quality assurance and cross check after
531 semi-automated lake mapping assure the quality of our lake dataset but are still time and cost
532 prohibitive. State-of-the-art mapping methods, such as deep learning method (Wu et al.,
533 2020), Google Earth Engine cloud-computing (Chen et al., 2021) and synergy of SAR and

534 optical images (Wangchuk and Bolch, 2020; How et al., 2021), would be used in the future to
535 balance product accuracy and time cost.

536 The glacial lake dataset will be updated using newly collected Landsat and Sentinel
537 images at a five-year interval or modified according to user feedbacks. The updated glacial
538 lake dataset will continue to be released freely and publicly on the Mountain Science Data
539 Center sharing platform.

540 **7 Data availability**

541 Our glacial lake dataset extracted from Sentinel-2 images in 2020 and Landsat observation
542 between 1990 and 2020 are available online via the Mountain Science Data Center, the
543 Institute of Mountain Hazards and Environment, the Chinese Academy of Sciences at
544 <https://doi.org/10.12380/Glaci.msdc.000001> (Lesi et al., 2022). The glacial lake dataset is
545 provided in both ESRI shapefile format (total size of 22.6 MB) and the Geopackage format
546 (version 1.2.1) with a total size of 9.2MB, which can be opened and further processed by
547 open-source geographic information system software such as QGIS.

548 **8 Conclusions**

549 Glacial lake inventories of the entire China-Pakistan Economic Corridor in 2020 were
550 provided based on Landsat and Sentinel-2 images using a threshold-based semi-automated
551 mapping method. Both Landsat and Sentinel-2 derived glacial lake dataset show similar
552 characteristics in spatial distribution and in the statistics of count and area. By contrast,
553 glacial lake dataset derived from Sentinel-2 images with a spatial resolution of 10 m has a
554 lower mapping error and more accurate lake boundary than those from 30 m spatial
555 resolution Landsat images whereas Landsat imagery is more suitable to analyze spatial-
556 temporal changes at a longer time scale due to its long-term archived observations at a
557 consistent 30 m spatial resolution starting from the late 1980s.

558 Glacial lakes in the study area remain relatively stable with a slight increase in number and
559 area between 1990 and 2020 according to Landsat observations. Our dataset reveals that 2154
560 glacial lakes in 1990 covering $85.1 \pm 14.66 \text{ km}^2$ increased to 2234 lakes with a total area of
561 $86.31 \pm 14.98 \text{ km}^2$. The same mapping method and rigorous workflow of quality assurance
562 and quality control used in this study reduced the error in multi-temporal changes of glacial
563 lakes.

564 The Hanshaw's error estimation method for pixel-based lake mapping was improved by
565 removing repeatedly calculated edge pixels that vary with lake shape. Therefore, the newly
566 proposed method reduces the estimated value of uncertainty from satellite observations. The
567 average relative error is $\pm 17.36\%$ for Landsat-derived product and $\pm 8.15\%$ for product from
568 Sentinel-2.

569 Our glacial lake dataset contains a range of critical parameters that maximize their
570 potential utility for water resource and GLOFs risk evaluation, cryosphere-hydrological and
571 glacier-lake evolution projection. The dual classification systems of glacial lake types were
572 developed and are very likely to attract broader researchers and scientists to use our datasets.
573 In comparison with other existing glacial lake datasets, our products were created through a
574 thorough consideration of lake types, cross checks and rigorous quality assurance, and will be

575 updated and released continuously in the Mountain Science Data Center. As such, we expect
576 that our glacial lake dataset will have significant value to cryospheric-hydrology research, the
577 assessment of water resource and glacier-related hazards in the CPEC.

578

579 **Appendix.** The appendix related to this article is available online.

580

581 **Author contributions.** ML and YN conceived the study, ML, YN and XD performed data
582 processing and analysis of the glacial lake inventory data, JW contributed to tool
583 development and mapping methods, ML and YN wrote the manuscript. All authors reviewed
584 and edited the manuscript before submission.

585

586 **Competing interests.** The authors declare no conflict of interest.

587

588 **Acknowledgements.**

589 We are grateful for the editor Kenneth Mankoff and three anonymous referees for their
590 constructive comments that greatly help us to improve this manuscript. This study was
591 supported by the second Tibetan Plateau Scientific Expedition and Research Program (grant
592 2019QZKK0603), the National Natural Science Foundation of China (Grant Nos. 42171086,
593 41971153), the International Science & Technology Cooperation Program of China (No.
594 2018YFE0100100), the Chinese Academy of Sciences “Light of West China” and Natural
595 Sciences and Engineering Research Council of Canada (Grant No. DG-2020-04207).

596

597 **References**

598 Ashraf, A., Naz, R., Iqbal, M.B.: Altitudinal dynamics of glacial lakes under changing climate in the Hindu

599 Kush, Karakoram, and Himalaya ranges. *Geomorphology*, 283: 72-79,

600 <https://doi.org/10.1016/j.geomorph.2017.01.033>, 2017.

601 Azam, M.F., Kargel, J.S., Shea, J.M., Nepal, S., Haritashya, U.K., Srivastava, S., Maussion, F., Qazi, N.,

602 Chevallier, P., Dimri, A.P., Kulkarni, A.V., Cogley, J.G., Bahuguna, I.: Glaciohydrology of the Himalaya-

603 Karakoram. *Science*, 373: eabf3668, <https://doi.org/10.1126/science.abf3668>, 2021.

604 Battamo, A.Y., Varis, O., Sun, P., Yang, Y., Oba, B.T., Zhao, L.: Mapping socio-ecological resilience along the

605 seven economic corridors of the Belt and Road Initiative. *J. Clean. Prod.*, 309: 127341,

606 <https://doi.org/10.1016/j.jclepro.2021.127341>, 2021.

607 Bhambri, R., Hewitt, K., Kawishwar, P., Kumar, A., Verma, A., Snehmani, Tiwari, S., Misra, A.: Ice-dams,

608 outburst floods, and movement heterogeneity of glaciers, Karakoram. *Global Planet. Change*, 180: 100-116,
609 <https://doi.org/10.1016/j.gloplacha.2019.05.004>, 2019.

610 Bhattacharya, A., Bolch, T., Mukherjee, K., King, O., Menounos, B., Kapitsa, V., Neckel, N., Yang, W., Yao,
611 T.: High Mountain Asian glacier response to climate revealed by multi-temporal satellite observations since the
612 1960s. *Nat. Commun.*, 12: 4133, <https://doi.org/10.1038/s41467-021-24180-y>, 2021.

613 Bolch, T., Pieczonka, T., Mukherjee, K., Shea, J.: Brief communication: Glaciers in the Hunza catchment
614 (Karakoram) have been nearly in balance since the 1970s. *The Cryosphere*, 11: 531-539,
615 <https://doi.org/10.5194/tc-11-531-2017>, 2017.

616 Brun, F., Berthier, E., Wagnon, P., Kääb, A., Treichler, D.: A spatially resolved estimate of High Mountain Asia
617 glacier mass balances from 2000 to 2016. *Nat. Geosci.*, 10: 668-673, <https://doi.org/10.1038/ngeo2999>, 2017.

618 Brun, F., Wagnon, P., Berthier, E., Jomelli, V., Maharjan, S.B., Shrestha, F., Kraaijenbrink, P.D.A.:
619 Heterogeneous Influence of Glacier Morphology on the Mass Balance Variability in High Mountain Asia. *J.*
620 *Geophys. Res-Earth*, 124: 1331-1345, <https://doi.org/10.1029/2018JF004838>, 2019.

621 Carrivick, J.L., Tweed, F.S.: Proglacial lakes: character, behaviour and geological importance. *Quaternary Sci.*
622 *Rev.*, 78: 34-52, <https://doi.org/10.1016/j.quascirev.2013.07.028>, 2013.

623 Carrivick, J.L., Quincey, D.J.: Progressive increase in number and volume of ice-marginal lakes on the western
624 margin of the Greenland Ice Sheet. *Global Planet. Change*, 116: 156-163,
625 <https://doi.org/10.1016/j.gloplacha.2014.02.009>, 2014.

626 Carrivick, J.L., Tweed, F.S.: A global assessment of the societal impacts of glacier outburst floods. *Global*
627 *Planet. Change*, 144: 1-16, <https://doi.org/10.1016/j.gloplacha.2016.07.001>, 2016.

628 Carrivick, J.L., Tweed, F.S., Sutherland, J.L., Mallalieu, J.: Toward Numerical Modeling of Interactions
629 Between Ice-Marginal Proglacial Lakes and Glaciers. *Front. Earth Sci.*, 8,

630 <https://doi.org/10.3389/feart.2020.577068>, 2020.

631 Carrivick, J.L., How, P., Lea, J.M., Sutherland, J.L., Grimes, M., Tweed, F.S., Cornford, S., Quincey, D.J.,
632 Mallalieu, J.: Ice-Marginal Proglacial Lakes Across Greenland: Present Status and a Possible Future. *Geophys.*
633 *Res. Lett.*, 49: e2022GL099276, <https://doi.org/https://doi.org/10.1029/2022GL099276>, 2022.

634 Chen, F., Zhang, M., Guo, H., Allen, S., Kargel, J.S., Haritashya, U.K., Watson, C.S.: Annual 30 m dataset for
635 glacial lakes in High Mountain Asia from 2008 to 2017. *Earth System Science Data*, 13: 741-766,
636 <https://doi.org/10.5194/essd-13-741-2021>, 2021.

637 Chen, X., Cui, P., You, Y., Cheng, Z., Khan, A., Ye, C., Zhang, S.: Dam-break risk analysis of the Attabad
638 landslide dam in Pakistan and emergency countermeasures. *Landslides*, 14: 675-683,
639 <https://doi.org/10.1007/s10346-016-0721-7>, 2017.

640 Cook, S.J., Quincey, D.J.: Estimating the volume of Alpine glacial lakes. *Earth Surf. Dynam.*, 3: 559-575,
641 <https://doi.org/10.5194/esurf-3-559-2015>, 2015.

642 Emmer, A., Cuřín, V.: Can a dam type of an alpine lake be derived from lake geometry? A negative result. *J.*
643 *Mt. Sci.-Engl.*, 18: 614-621, <https://doi.org/10.1007/s11629-020-6003-9>, 2021.

644 Farr, T.G., Rosen, P.A., Caro, E., Crippen, R., Duren, R., Hensley, S., Kobrick, M., Paller, M., Rodriguez, E.,
645 Roth, L., Seal, D., Shaffer, S., Shimada, J., Umland, J., Werner, M., Oskin, M., Burbank, D., Alsdorf, D.: The
646 Shuttle Radar Topography Mission. *Rev. Geophys.*, 45: RG2004, <https://doi.org/10.1029/2005RG000183>, 2007.

647 Gardelle, J., Arnaud, Y., Berthier, E.: Contrasted evolution of glacial lakes along the Hindu Kush Himalaya
648 mountain range between 1990 and 2009. *Global Planet. Change*, 75: 47-55,
649 <https://doi.org/10.1016/j.gloplacha.2010.10.003>, 2011.

650 Hanshaw, M.N., Bookhagen, B.: Glacial areas, lake areas, and snow lines from 1975 to 2012: status of the
651 Cordillera Vilcanota, including the Quelccaya Ice Cap, northern central Andes, Peru. *The Cryosphere*, 8: 359-

652 376, <https://doi.org/10.5194/tc-8-359-2014>, 2014.

653 Hewitt, K.: The Karakoram Anomaly? Glacier Expansion and the ‘Elevation Effect,’ Karakoram Himalaya. *Mt.*
654 *Res. Dev.*, 25: 332-340, [https://doi.org/10.1659/0276-4741\(2005\)025\[0332:TKAGEA\]2.0.CO;2](https://doi.org/10.1659/0276-4741(2005)025[0332:TKAGEA]2.0.CO;2), 2005.

655 Hewitt, K., 2014. *Glaciers of the Karakoram Himalaya: Glacial Environments, Processes, Hazards and*
656 *Resources*. Springer, Dordrecht.

657 How, P., Messerli, A., Mätzler, E., Santoro, M., Wiesmann, A., Caduff, R., Langley, K., Bojesen, M.H., Paul,
658 F., Kääb, A., Carrivick, J.L.: Greenland-wide inventory of ice marginal lakes using a multi-method approach.
659 *Sci. Rep.-UK*, 11: 4481, <https://doi.org/10.1038/s41598-021-83509-1>, 2021.

660 Huggel, C., Kääb, A., Haeberli, W., Teysseire, P., Paul, F.: Remote sensing based assessment of hazards from
661 glacier lake outbursts: a case study in the Swiss Alps. *Can. Geotech. J.*, 39: 316-330,
662 <https://doi.org/10.1139/t01-099>, 2002.

663 Hugonnet, R., McNabb, R., Berthier, E., Menounos, B., Nuth, C., Girod, L., Farinotti, D., Huss, M., Dussaillant,
664 I., Brun, F., Kääb, A.: Accelerated global glacier mass loss in the early twenty-first century. *Nature*, 592: 726-
665 731, <https://doi.org/10.1038/s41586-021-03436-z>, 2021.

666 Huss, M., Hock, R.: Global-scale hydrological response to future glacier mass loss. *Nat. Clim. Change*, 8: 135-
667 140, <https://doi.org/10.1038/s41558-017-0049-x>, 2018.

668 Immerzeel, W.W., Lutz, A.F., Andrade, M., Bahl, A., Biemans, H., Bolch, T., Hyde, S., Brumby, S., Davies,
669 B.J., Elmore, A.C., Emmer, A., Feng, M., Fernández, A., Haritashya, U., Kargel, J.S., Koppes, M.,
670 Kraaijenbrink, P.D.A., Kulkarni, A.V., Mayewski, P.A., Nepal, S., Pacheco, P., Painter, T.H., Pellicciotti, F.,
671 Rajaram, H., Rupper, S., Sinisalo, A., Shrestha, A.B., Viviroli, D., Wada, Y., Xiao, C., Yao, T., Baillie, J.E.M.:
672 Importance and vulnerability of the world’s water towers. *Nature*, 577: 364-369, [https://doi.org/10.1038/s41586-](https://doi.org/10.1038/s41586-019-1822-y)
673 [019-1822-y](https://doi.org/10.1038/s41586-019-1822-y), 2020.

674 Jarvis, A., Reuter, H.I., Nelson, A., Guevara, E., 2008. Hole-filled seamless SRTM data V4. 2008, International
675 Centre for Tropical Agriculture (CIAT), available from <http://srtm.csi.cgiar.org>.

676 Jiang, S., Nie, Y., Liu, Q., Wang, J., Liu, L., Hassan, J., Liu, X., Xu, X.: Glacier Change, Supraglacial Debris
677 Expansion and Glacial Lake Evolution in the Gyirong River Basin, Central Himalayas, between 1988 and 2015.
678 *Remote Sens.-Basel*, 10: 986, <https://doi.org/10.3390/rs10070986>, 2018.

679 Kääb, A., Berthier, E., Nuth, C., Gardelle, J., Arnaud, Y.: Contrasting patterns of early twenty-first-century
680 glacier mass change in the Himalayas. *Nature*, 488: 495-498, <https://doi.org/10.1038/nature11324>, 2012.

681 Lesi, M., Nie, Y., Shugar, D.H., Wang, J., Deng, Q., Chen, H.: Landsat and Sentinel-derived glacial lake dataset
682 in the China-Pakistan Economic Corridor from 1990 to 2020. Mountain Science Data Center,
683 <https://doi.org/10.12380/Glaci.msdc.000001> CSTR:1a006.11.Glaci.msdc.000001, 2022.

684 Li, D., Shanguan, D., Anjum, M.N.: Glacial Lake Inventory Derived from Landsat 8 OLI in 2016–2018 in
685 China–Pakistan Economic Corridor. *ISPRS international journal of geo-information*, 9: 294,
686 <https://doi.org/10.3390/ijgi9050294>, 2020.

687 Li, Z., Deng, X., Zhang, Y.: Evaluation and convergence analysis of socio-economic vulnerability to natural
688 hazards of Belt and Road Initiative countries. *J. Clean. Prod.*, 282: 125406,
689 <https://doi.org/10.1016/j.jclepro.2020.125406>, 2021.

690 Liu, Q., Mayer, C.: Distribution and interannual variability of supraglacial lakes on debris-covered glaciers in
691 the Khan Tengri-Tumor Mountains, Central Asia. *Environ. Res. Lett.*, 10: 014014 2015.

692 Liu, Q., Mayer, C., Wang, X., Nie, Y., Wu, K., Wei, J., Liu, S.: Interannual flow dynamics driven by frontal
693 retreat of a lake-terminating glacier in the Chinese Central Himalaya. *Earth Planet. Sc. Lett.*, 546: 116450,
694 <https://doi.org/10.1016/j.epsl.2020.116450>, 2020.

695 Lyons, E.A., Sheng, Y., Smith, L.C., Li, J., Hinkel, K.M., Lenters, J.D., Wang, J.: Quantifying sources of error

696 in multitemporal multisensor lake mapping. *Int. J. Remote Sens.*, 34: 7887-7905,
697 <https://doi.org/10.1080/01431161.2013.827343>, 2013.

698 Mankoff, K.D., Noël, B., Fettweis, X., Ahlstrøm, A.P., Colgan, W., Kondo, K., Langley, K., Sugiyama, S., van
699 As, D., Fausto, R.S.: Greenland liquid water discharge from 1958 through 2019. *Earth Syst. Sci. Data*, 12: 2811-
700 2841, <https://doi.org/10.5194/essd-12-2811-2020>, 2020.

701 Martín, C.N.S., Ponce, J.F., Montes, A., Balocchi, L.D., Gorza, C., Andrea, C.: Proglacial landform assemblage
702 in a rapidly retreating cirque glacier due to temperature increase since 1970, Fuegian Andes, Argentina.
703 *Geomorphology*, 390: 107861, <https://doi.org/10.1016/j.geomorph.2021.107861>, 2021.

704 Maurer, J.M., Schaefer, J.M., Rupper, S., Corley, A.: Acceleration of ice loss across the Himalayas over the past
705 40 years. *Sci. Adv.*, 5: eaav7266, <https://doi.org/10.1126/sciadv.aav7266>, 2019.

706 Mcfeeters, S.K.: The use of the Normalized Difference Water Index (NDWI) in the delineation of open water
707 features. *Int. J. Remote Sens.*, 17: 1425 - 1432 1996.

708 Miles, E.S., Watson, C.S., Brun, F., Berthier, E., Esteves, M., Quincey, D.J., Miles, K.E., Hubbard, B., Wagnon,
709 P.: Glacial and geomorphic effects of a supraglacial lake drainage and outburst event, Everest region, Nepal
710 Himalaya. *The Cryosphere*, 12: 3891-3905, <https://doi.org/10.5194/tc-12-3891-2018>, 2018.

711 Nie, Y., Zhang, Y., Liu, L., Zhang, J.: Glacial change in the vicinity of Mt. Qomolangma (Everest), central high
712 Himalayas since 1976. *J. Geogr. Sci.*, 20: 667-686, <https://doi.org/10.1007/s11442-010-0803-8>, 2010.

713 Nie, Y., Sheng, Y., Liu, Q., Liu, L., Liu, S., Zhang, Y., Song, C.: A regional-scale assessment of Himalayan
714 glacial lake changes using satellite observations from 1990 to 2015. *Remote Sens. Environ.*, 189: 1-13,
715 <https://doi.org/10.1016/j.rse.2016.11.008>, 2017.

716 Nie, Y., Liu, Q., Wang, J., Zhang, Y., Sheng, Y., Liu, S.: An inventory of historical glacial lake outburst floods
717 in the Himalayas based on remote sensing observations and geomorphological analysis. *Geomorphology*, 308:

718 91-106, <https://doi.org/10.1016/j.geomorph.2018.02.002>, 2018.

719 Nie, Y., Liu, W., Liu, Q., Hu, X., Westoby, M.J.: Reconstructing the Chongbaxia Tsho glacial lake outburst
720 flood in the Eastern Himalaya: Evolution, process and impacts. *Geomorphology*, 370: 107393,
721 <https://doi.org/10.1016/j.geomorph.2020.107393>, 2020.

722 Nie, Y., Pritchard, H.D., Liu, Q., Hennig, T., Wang, W., Wang, X., Liu, S., Nepal, S., Samyn, D., Hewitt, K.,
723 Chen, X.: Glacial change and hydrological implications in the Himalaya and Karakoram. *Nature Reviews Earth
724 & Environment*, 2: 91-106, <https://doi.org/10.1038/s43017-020-00124-w>, 2021.

725 Paul, F., Rastner, P., Azzoni, R.S., Diolaiuti, G., Fugazza, D., Le Bris, R., Nemec, J., Rabatel, A., Ramusovic,
726 M., Schwaizer, G., Smiraglia, C.: Glacier shrinkage in the Alps continues unabated as revealed by a new glacier
727 inventory from Sentinel-2. *Earth System Science Data*, 12: 1805-1821, [https://doi.org/10.5194/essd-12-1805-](https://doi.org/10.5194/essd-12-1805-2020)
728 2020, 2020.

729 Pfeffer, W.T., Arendt, A.A., Bliss, A., Bolch, T., Cogley, J.G., Gardner, A.S., Hagen, J., Hock, R., Kaser, G.,
730 Kienholz, C., Miles, E.S., Moholdt, G., Mölg, N., Paul, F., Radić, V., Rastner, P., Raup, B.H., Rich, J., Sharp,
731 M.J.: The Randolph Glacier Inventory: a globally complete inventory of glaciers. *J. Glaciol.*, 60: 537-552,
732 <https://doi.org/10.3189/2014JoG13J176>, 2014.

733 Post, A., Mayo, L.R., 1971. Glacier dammed lakes and outburst floods in Alaska: U.S. Geological Survey
734 Hydrologic Investigations Atlas 455, U.S. Geological Survey.

735 Pritchard, H.D.: Asia's shrinking glaciers protect large populations from drought stress. *Nature*, 569: 649-654,
736 <https://doi.org/10.1038/s41586-019-1240-1>, 2019.

737 Quincey, D.J., Richardson, S.D., Luckman, A., Lucas, R.M., Reynolds, J.M., Hambrey, M.J., Glasser, N.F.:
738 Early recognition of glacial lake hazards in the Himalaya using remote sensing datasets. *Global Planet. Change*,
739 56: 137-152, <https://doi.org/10.1016/j.gloplacha.2006.07.013>, 2007.

740 Rabus, B., Eineder, M., Roth, A., Bamler, R.: The shuttle radar topography mission—a new class of digital
741 elevation models acquired by spaceborne radar. *ISPRS J. Photogramm.*, 57: 241-262,
742 [https://doi.org/10.1016/S0924-2716\(02\)00124-7](https://doi.org/10.1016/S0924-2716(02)00124-7), 2003.

743 RGI Consortium: Randolph Glacier Inventory – A Dataset of Global Glacier Outlines: Version 6.0: Technical
744 Report, <https://doi.org/10.7265/N5-RGI-60>, 2017.

745 Rick, B., Mcgrath, D., Armstrong, W., Mccoy, S.W.: Dam type and lake location characterize ice-marginal lake
746 area change in Alaska and NW Canada between 1984 and 2019. *The Cryosphere*, 16: 297-314,
747 <https://doi.org/10.5194/tc-16-297-2022>, 2022.

748 Rose, A., Mckee, J., Sims, K., Bright, E., Reith, A., Urban, M.: LandScan Global 2020,
749 <https://doi.org/https://doi.org/10.48690/1523378>, 2021.

750 Rounce, D.R., Hock, R., Shean, D.E.: Glacier Mass Change in High Mountain Asia Through 2100 Using the
751 Open-Source Python Glacier Evolution Model (PyGEM). *Front. Earth Sci*, 7: 331,
752 <https://doi.org/10.3389/feart.2019.00331>, 2020.

753 Roy, D.P., Wulder, M.A., Loveland, T.R., C. E., W., Allen, R.G., Anderson, M.C., Helder, D., Irons, J.R.,
754 Johnson, D.M., Kennedy, R., Scambos, T.A., Schaaf, C.B., Schott, J.R., Sheng, Y., Vermote, E.F., Belward,
755 A.S., Bindschadler, R., Cohen, W.B., Gao, F., Hipple, J.D., Hostert, P., Huntington, J., Justice, C.O., Kilic, A.,
756 Kovalskyy, V., Lee, Z.P., Lymburner, L., Masek, J.G., Mccorkel, J., Shuai, Y., Trezza, R., Vogelmann, J.,
757 Wynne, R.H., Zhu, Z.: Landsat-8: Science and product vision for terrestrial global change research. *Remote*
758 *Sens. Environ.*, 145: 154-172, <https://doi.org/10.1016/j.rse.2014.02.001>, 2014.

759 Sakai, A.: Brief communication: Updated GAMDAM glacier inventory over high-mountain Asia. *The*
760 *Cryosphere*, 13: 2043-2049, <https://doi.org/10.5194/tc-13-2043-2019>, 2019.

761 Salerno, F., Thakuri, S., D'Agata, C., Smiraglia, C., Manfredi, E.C., Viviano, G., Tartari, G.: Glacial lake

762 distribution in the Mount Everest region: Uncertainty of measurement and conditions of formation. *Global*
763 *Planet. Change*, 92-93: 30-39 2012.

764 Shean, D.E., Bhushan, S., Montesano, P., Rounce, D.R., Arendt, A., Osmanoglu, B.: A Systematic, Regional
765 Assessment of High Mountain Asia Glacier Mass Balance. *Front. Earth Sci*, 7: 363,
766 <https://doi.org/10.3389/feart.2019.00363>, 2020.

767 Sheng, Y., Song, C., Wang, J., Lyons, E.A., Knox, B.R., Cox, J.S., Gao, F.: Representative lake water extent
768 mapping at continental scales using multi-temporal Landsat-8 imagery. *Remote Sens. Environ.*, 185: 129-141,
769 <https://doi.org/10.1016/j.rse.2015.12.041>, 2016.

770 Shugar, D.H., Burr, A., Haritashya, U.K., Kargel, J.S., Watson, C.S., Kennedy, M.C., Bevington, A.R., Betts,
771 R.A., Harrison, S., Strattman, K.: Rapid worldwide growth of glacial lakes since 1990. *Nat. Clim. Change*, 10:
772 939-945, <https://doi.org/10.1038/s41558-020-0855-4>, 2020.

773 Shugar, D.H., Jacquemart, M., Shean, D., Bhushan, S., Upadhyay, K., Sattar, A., Schwanghart, W., McBride, S.,
774 de Vries, M., Mergili, M., Emmer, A., Deschamps-Berger, C., McDonnell, M., Bhambri, R., Allen, S., Berthier,
775 E., Carrivick, J.L., Clague, J.J., Dokukin, M., Dunning, S.A., Frey, H., Gascoïn, S., Haritashya, U.K., Huggel,
776 C., Kaab, A., Kargel, J.S., Kavanaugh, J.L., Lacroix, P., Petley, D., Rupper, S., Azam, M.F., Cook, S.J., Dimri,
777 A.P., Eriksson, M., Farinotti, D., Fiddes, J., Gnyawali, K.R., Harrison, S., Jha, M., Koppes, M., Kumar, A.,
778 Leinss, S., Majeed, U., Mal, S., Muhuri, A., Noetzli, J., Paul, F., Rashid, I., Sain, K., Steiner, J., Ugalde, F.,
779 Watson, C.S., Westoby, M.J.: A massive rock and ice avalanche caused the 2021 disaster at Chamoli, Indian
780 Himalaya. *Science*, 373: 300-306, <https://doi.org/10.1126/science.abh4455>, 2021.

781 Ullah, S., You, Q., Ali, A., Ullah, W., Jan, M.A., Zhang, Y., Xie, W., Xie, X.: Observed changes in maximum
782 and minimum temperatures over China- Pakistan economic corridor during 1980–2016. *Atmos. Res.*, 216: 37-
783 51, <https://doi.org/10.1016/j.atmosres.2018.09.020>, 2019.

784 Viviroli, D., Kummu, M., Meybeck, M., Kallio, M., Wada, Y.: Increasing dependence of lowland populations
785 on mountain water resources. *Nature Sustainability*, 3: 917-928, <https://doi.org/10.1038/s41893-020-0559-9>,
786 2020.

787 Wang, J., Sheng, Y., Tong, T.S.D.: Monitoring decadal lake dynamics across the Yangtze Basin downstream of
788 Three Gorges Dam. *Remote Sens. Environ.*, 152: 251-269, <https://doi.org/10.1016/j.rse.2014.06.004>, 2014.

789 Wang, J., Sheng, Y., Wada, Y.: Little impact of the Three Gorges Dam on recent decadal lake decline across
790 China's Yangtze Plain. *Water Resour. Res.*, 53: 3854-3877, <https://doi.org/10.1002/2016WR019817>, 2017.

791 Wang, J., Song, C., Reager, J.T., Yao, F., Famiglietti, J.S., Sheng, Y., Macdonald, G.M., Brun, F., Schmied,
792 H.M., Marston, R.A., Wada, Y.: Recent global decline in endorheic basin water storages. *Nat. Geosci.*, 11: 926-
793 932, <https://doi.org/10.1038/s41561-018-0265-7>, 2018.

794 Wang, X., Ding, Y., Liu, S., Jiang, L., Wu, K., Jiang, Z., Guo, W.: Changes of glacial lakes and implications in
795 Tian Shan, Central Asia, based on remote sensing data from 1990 to 2010. *Environ. Res. Lett.*, 8: 44052,
796 <https://doi.org/10.1088/1748-9326/8/4/044052>, 2013.

797 Wang, X., Liu, S., Zhang, J.: A new look at roles of the cryosphere in sustainable development. *Advances in*
798 *Climate Change Research*, 10: 124-131, <https://doi.org/10.1016/j.accre.2019.06.005>, 2019.

799 Wang, X., Guo, X., Yang, C., Liu, Q., Wei, J., Zhang, Y., Liu, S., Zhang, Y., Jiang, Z., Tang, Z.: Glacial lake
800 inventory of high-mountain Asia in 1990 and 2018 derived from Landsat images. *Earth System Science Data*,
801 12: 2169-2182, <https://doi.org/10.5194/essd-12-2169-2020>, 2020.

802 Wangchuk, S., Bolch, T.: Mapping of glacial lakes using Sentinel-1 and Sentinel-2 data and a random forest
803 classifier: Strengths and challenges. *Science of Remote Sensing*, 2: 100008,
804 <https://doi.org/https://doi.org/10.1016/j.srs.2020.100008>, 2020.

805 Westoby, M.J., Glasser, N.F., Brasington, J., Hambrey, M.J., Quincey, D.J., Reynolds, J.M.: Modelling outburst

806 floods from moraine-dammed glacial lakes. *Earth-Sci. Rev.*, 134: 137-159,
807 <https://doi.org/10.1016/j.earscirev.2014.03.009>, 2014.

808 Williamson, A.G., Banwell, A.F., Willis, I.C., Arnold, N.S.: Dual-satellite (Sentinel-2 and Landsat 8) remote
809 sensing of supraglacial lakes in Greenland. *The Cryosphere*, 12: 3045-3065, [https://doi.org/10.5194/tc-12-3045-](https://doi.org/10.5194/tc-12-3045-2018)
810 2018, 2018.

811 Wu, R., Liu, G., Zhang, R., Wang, X., Li, Y., Zhang, B., Cai, J., Xiang, W.: A Deep Learning Method for
812 Mapping Glacial Lakes from the Combined Use of Synthetic-Aperture Radar and Optical Satellite Images.
813 *Remote Sens.-Basel*, 12: 4020
814 2020.

815 Wulder, M.A., Loveland, T.R., Roy, D.P., Crawford, C.J., Masek, J.G., Woodcock, C.E., Allen, R.G.,
816 Anderson, M.C., Belward, A.S., Cohen, W.B., Dwyer, J., Erb, A., Gao, F., Griffiths, P., Helder, D., Hermosilla,
817 T., Hipple, J.D., Hostert, P., Hughes, M.J., Huntington, J., Johnson, D.M., Kennedy, R., Kilic, A., Li, Z.,
818 Lymburner, L., Mccorkel, J., Pahlevan, N., Scambos, T.A., Schaaf, C., Schott, J.R., Sheng, Y., Storey, J.,
819 Vermote, E., Vogelmann, J., White, J.C., Wynne, R.H., Zhu, Z.: Current status of Landsat program, science, and
820 applications. *Remote Sens. Environ.*, 225: 127-147, <https://doi.org/https://doi.org/10.1016/j.rse.2019.02.015>,
821 2019.

822 Yao, C., Wang, X., Zhao, X., Wei, J., Zhang, Y.: Temporal and Spatial Changes of Glacial Lakes in the China-
823 Pakistan Economic Corridor from 1990 to 2018. *Journal of Glaciology and Geocryology*, 42: 33-42,
824 <https://doi.org/https://doi.org/10.7522/j.issn.1000-0240.2020.0009>, 2020.

825 Yao, T., Thompson, L., Yang, W., Yu, W.S., Gao, Y., Guo, X.J., Yang, X.X., Duan, K.Q., Zhao, H.B., Xu,
826 B.Q., Pu, J.C., Lu, A.X., Xiang, Y., Kattel, D.B., Joswiak, D.: Different glacier status with atmospheric
827 circulations in Tibetan Plateau and surroundings. *Nat. Clim. Change*, 2: 663-667,

828 <https://doi.org/10.1038/NCLIMATE1580>, 2012.

829 Yao, X., Liu, S., Han, L., Sun, M., Zhao, L.: Definition and classification system of glacial lake for inventory
830 and hazards study. *J. Geogr. Sci.*, 28: 193-205, <https://doi.org/10.1007/s11442-018-1467-z>, 2018.

831 Zhang, G., Yao, T., Xie, H., Wang, W., Yang, W.: An inventory of glacial lakes in the Third Pole region and
832 their changes in response to global warming. *Global Planet. Change*, 131: 148-157,
833 <https://doi.org/10.1016/j.gloplacha.2015.05.013>, 2015.

834 Zhang, M., Chen, F., Tian, B.: An automated method for glacial lake mapping in High Mountain Asia using
835 Landsat 8 imagery. *J. Mt. Sci.-Engl.*, 15: 13-24, <https://doi.org/10.1007/s11629-017-4518-5>, 2018.

836 Zhao, W., Xiong, D., Wen, F., Wang, X.: Lake area monitoring based on land surface temperature in the Tibetan
837 Plateau from 2000 to 2018. *Environ. Res. Lett.*, 15, <https://doi.org/10.1088/1748-9326/ab9b41>, 2020.

838 Zheng, G., Allen, S.K., Bao, A., Ballesteros-Cánovas, J.A., Huss, M., Zhang, G., Li, J., Yuan, Y., Jiang, L., Yu,
839 T., Chen, W., Stoffel, M.: Increasing risk of glacial lake outburst floods from future Third Pole deglaciation.
840 *Nat. Clim. Change*, 11: 411-417, <https://doi.org/10.1038/s41558-021-01028-3>, 2021.

841
842

843 **Appendix**

844 **Tutorial for Improved Uncertainty Estimating Method**

845
846 The Hanshaw’s equation was originally proposed for pixelated polygons (such as a polygon
847 directly extracted from a remote sensing image), and performed more robustly than manually
848 digitized polygons (where vertices do not necessarily follow the pixel edges). Our improved
849 method also performs better for pixelated polygons. This tutorial is dedicated to helping
850 implement our improved uncertainty estimation method.

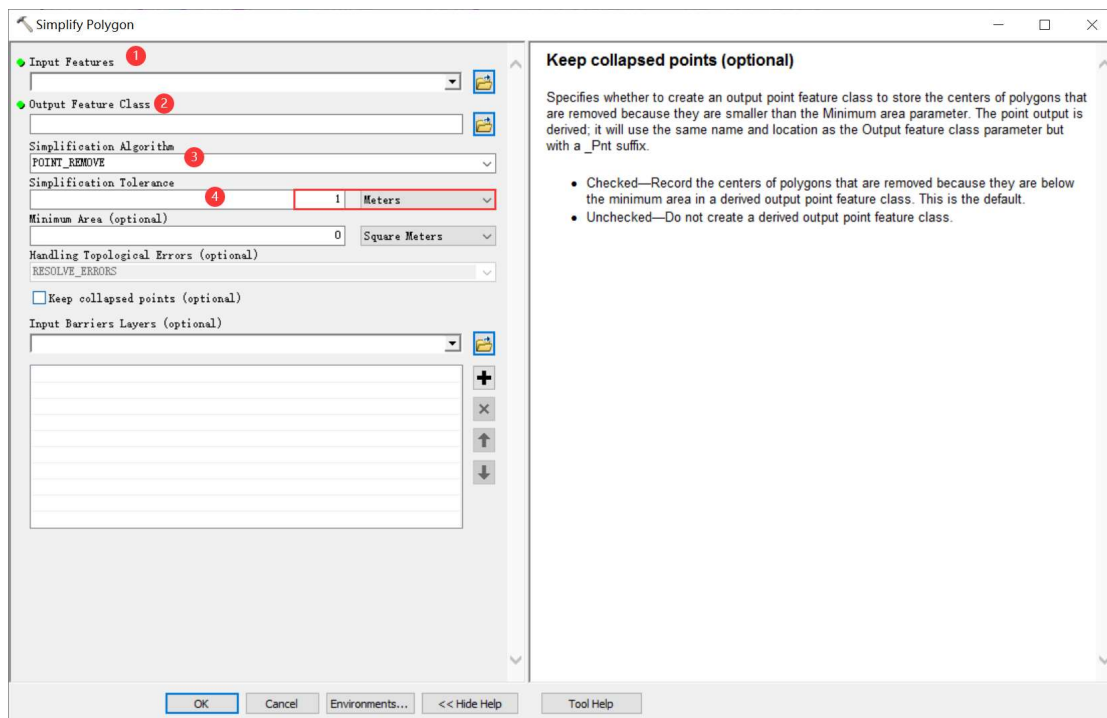
851
852 **Procedure of uncertainty estimating method (using ArcGIS (© ESRI) for example)**

853 1. Removing redundant nodes (optional)

854 We found that a small proportion (~1%) of the pixelated lake polygons (directly extracted
855 from satellite images) have redundant nodes, which affects the value of inner nodes. If no
856 redundant nodes exist, this step can be skipped. Or, we recommend using the “Simplify
857 Polygon” tool in ArcGIS to remove those nodes (Figure A1).

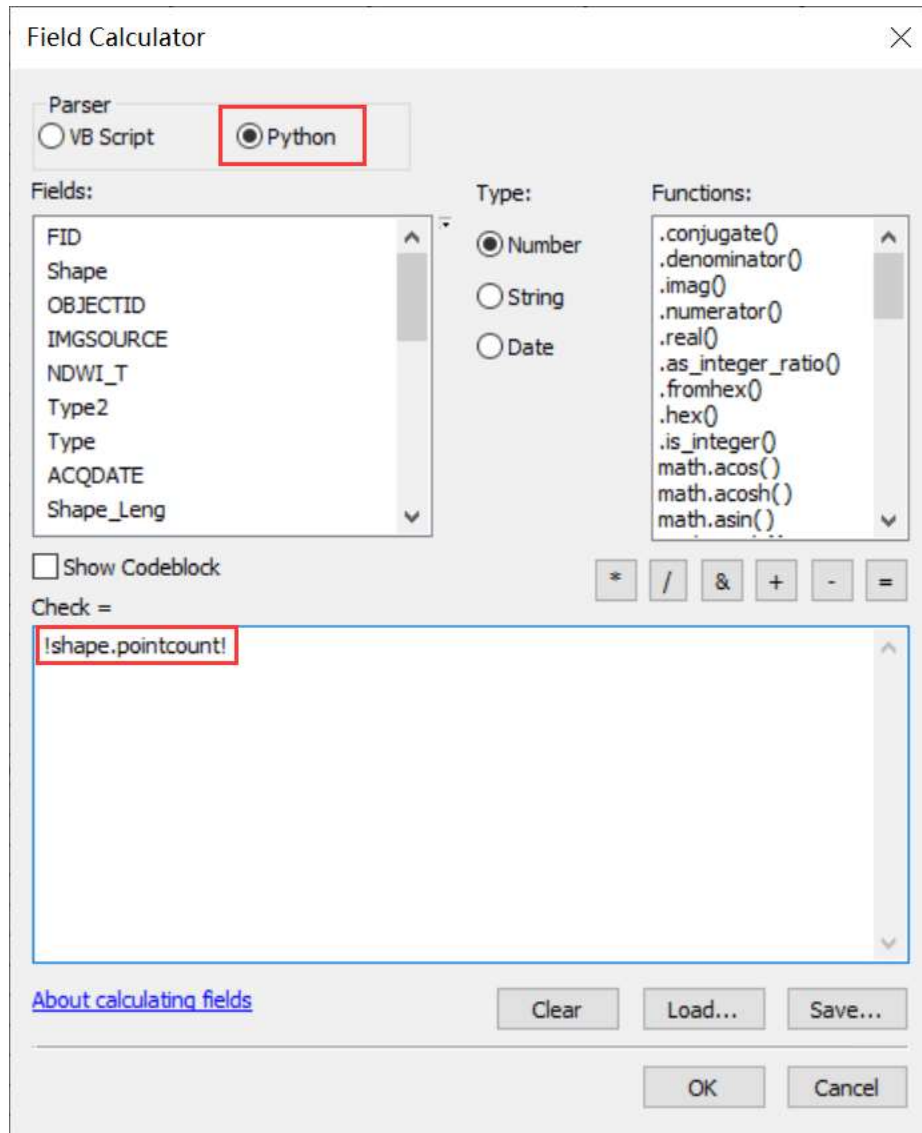
858 In the Simplify Polygon panel

- 859 • Input your dataset.
- 860 • Set the output path and output file name.
- 861 • Choose the simplification algorithm. We recommended “POINT_REMOVE”.
- 862 • Set the tolerance of simplification algorithm. In this step, we need to ensure that the
863 polygon boundaries remain unchanged after deleting redundant nodes. Generally, a
864 tolerance of 1 meter will suffice, or you can adjust the threshold until your satisfaction.



865
866 **Figure A1.** Input and option for Simplify Polygon in ArcGIS.
867

- 868 2. Calculating the total number of nodes using ArcGIS (Figure A2):
- 869 • Add a new field in the attribute table of dataset.
- 870 • Open Field Calculator.
- 871 • Switch the parser to python mode, and enter the following code “!shape.pointcount!” in
- 872 the blue box to calculate the total number of nodes for each glacial lake boundary.



873

874 **Figure A2.** Total node calculation in ArcGIS.

875

- 876 3. Calculating the number of inner nodes:
- 877

878 For polygons without islands (Figure A3), use the equation 5. An inner node is a polygon

879 vertex where the interior angle surrounding it is greater than 180 degrees. An outer node is

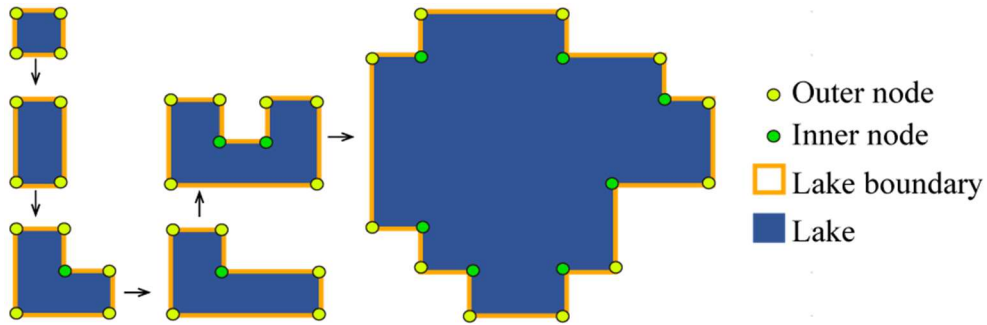
880 the opposite of the inner node, where the interior angle is less than 180 degrees. We found

881 that the outer nodes are usually four more than the inner nodes in our glacial lake dataset. The

882 total nodes in ArcGIS contain one overlapping node to close the polygon, meaning the

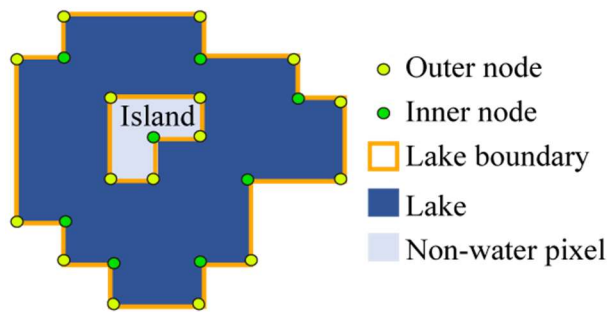
883 endpoint is also the startpoint. This extra count was deleted in the calculation (equation 5).

884



885
886 **Figure A3.** Sketch of outer and inner nodes of various glacial lakes without island.
887

888 For polygons with island (Figure A4) use the equation 6.
889

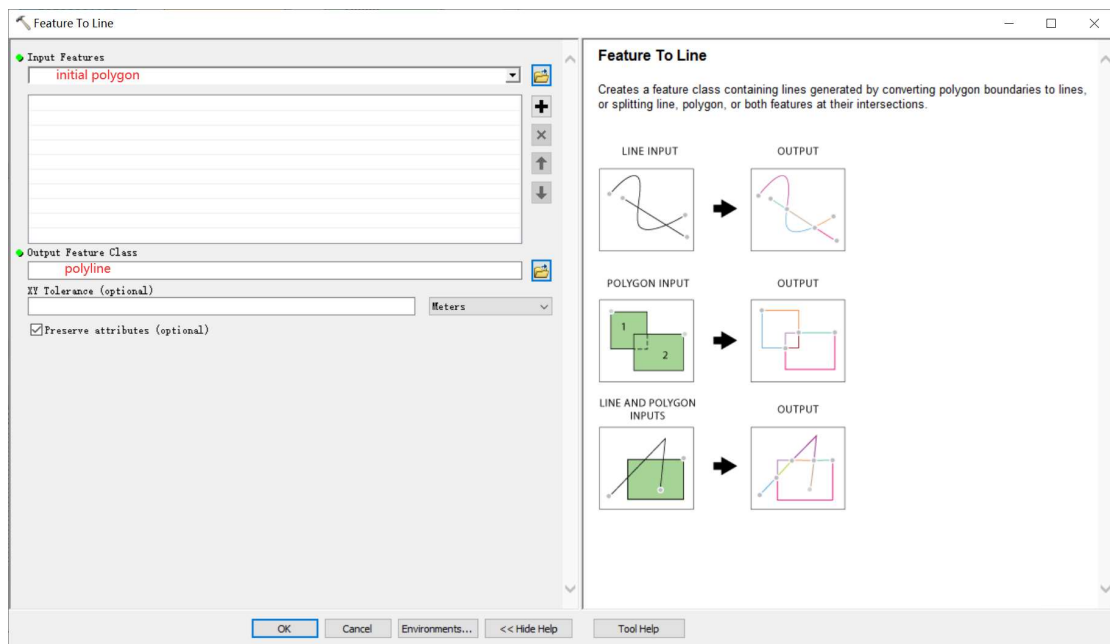


890
891 **Figure A4.** Sketch of outer and inner nodes for glacial lake with island.
892

893 We further specify the steps below to help implement equation 6.
894

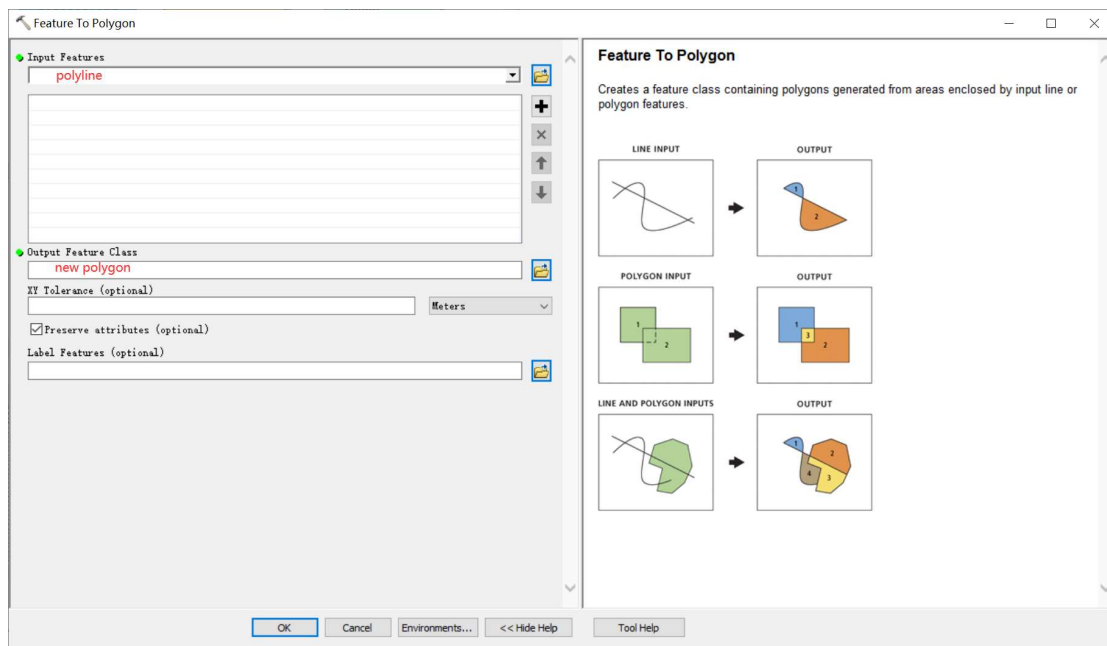
895 Sept 1: detect the number of islands within each polygon.
896

- Convert the initial lake polygon to polyline using the “Feature To Line” tool (Figure A5).



897
898 **Figure A5.** Feature To Line tool in ArcGIS
899

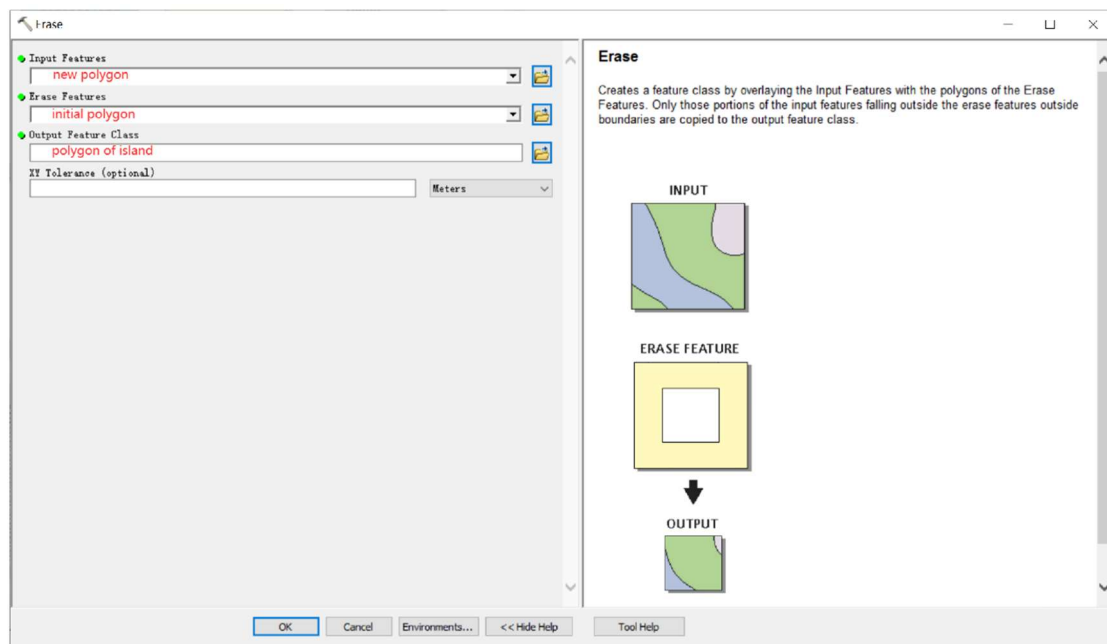
- 900 • Convert the polyline to generate a new polygon (Figure A6).



901
902
903
904
905

Figure A6. Feature To Polygon tool in ArcGIS

- Erase the new polygon by the initial polygon, which outputs the islands. Then we can count how many islands there are in each lake (Figure A7).



906
907
908
909
910
911
912

Figure A7. Erase tool in ArcGIS.

Step 2: calculate the number of inner nodes for each polygon with island using equation 6.

4. Calculating the uncertainty of lake mapping using equation 4.